Bennett Vorticity:
A family of nonlinear Shear-Flow Stabilized Z-pinch equilibria

Matt Russell

The Bennett profile is a classic form for the plasma number density of an equilibrium Z-pinch that has been studied for almost a century by plasma physicists interested in nonlinear plasma pinch science, and fusion energy. By transferring the nonlinearity entirely from the number density to the plasma flow velocity the current density of the resulting flowing Z-pinch equilibrium remains unchanged whilst now being defined by a vortical flow which previously did not exist in the classic case. Due to the positive-definite structure of the nonlinearity's first derivative, in the ideal limit this equilibrium conforms globally to the validity criterion for a shear-flow stabilized Z-pinch when the form of the temperature profile satisfies certain constraints. An analytic equilibrium can be found for the case $T = \frac{T_p}{r_p^3} r^3$, and is investigated. The predictions are found to be in good agreement where they should with the observations from the Zap, and Zap-HD DD fusion devices, including a very accurate prediction of the shear for FuZE-like conditions, and an axial profile that can be seen developing at multiple instances, due to the scaling of a smallness parameter. The minimum pinch length necessary for the pure-flow vortex to form an SFS equilibrium is found to be arbitrarily small arbitrarily close to the pinch axis. The observation of nonuniform density is explained by the mixing of the Bennett nonlinearity amongst the density and flow profiles because the cubic vortex current will give an analytic magnetic field.

INTRODUCTION

Bennett profiles[1][2] have historically described a class of Z-pinch equilibria who possess a nonlinear density profile,

$$n(r) = \frac{n_0}{(1+\xi^2 r^2)^2} \tag{1}$$

where following off of Bennett we can define,

$$\xi^2 = b n_0 \tag{2}$$

as a normalizing quantity with the dimension of an inverse length squared. The Bennett parameter for a two-fluid system,

$$b = \frac{\mu_0 e^2 u_0^2}{8 k_B (T_e + T_i)} \tag{3}$$

is a characteristic parameter describing a fluid plasma with separate temperatures for electrons and ions, and a uniform flow velocity, as well as a core plasma (number) density of n_0.

In the ideal limit, $R_m = \mu\sigma u L \to \infty$, and from a magnetohydrodynamic perspective this means that $T = T_e \simeq T_i$, so

$$b = \frac{\mu_0 e^2 u_0^2}{16 k_B T} = \frac{C_B}{T} = (1.45697 * 10^{-22}) \frac{u_{z,0}^2}{T} \tag{4}$$

Despite the presence of a $\sim \frac{1}{r^4}$ nonlinearity in the plasma density it turns out that the fluid equations of an ideal plasma, i.e., Ideal Magnetohydrodynamics (MHD) can be solved exactly in the case of an axisymmetric equilibrium. Meaning, here, one that is symmetric both azimuthally and axially, because the governing partial differential equations (PDE) describing the equilibrium reduce to an integrable system of ordinary differential equations (ODE) expressing the typical fluid conservation laws augmented by the appropriate form of Maxwell's equations.

This analytic nature to the classic Bennett Pinch is critical because it means that if we swap the density and flow profiles, i.e.,

$$n(r) \to n_0 \tag{5}$$

$$u_{z,0} \to u_z(r) = \frac{u_{z,0}}{(1+\xi^2 r^2)^2} \tag{6}$$

where $u_{z,0}$ is of course the amplitude of the core plasma flow, then the current density remains unchanged while now representing a flow state which is non-uniform, i.e., vortical.

This non-zero vorticity is more than just a mathematical curiosity. In the axisymmetric case, and for a purely axial flow, it naturally expresses a flow shear,

$$\vec{w} = \nabla \times \vec{u} = w_\theta \hat{\theta} = -\frac{\mathrm{d}u_z}{\mathrm{d}r} \hat{\theta} \tag{7}$$

This is relevant as modern fusion science enjoys the advantage of the Shear-Flow Stabilized Z-Pinch[3], which is a form of the Z-Pinch that can be stabilized against the $m = 0$, and $m = 1$ instabilities naturally plaguing the device[4][5]. When the flow shear is great enough, a quasi-equilibrium appears which is stable for several orders of magnitude longer than the predicted lifetime of a static Z-pinch[6][7], and which evidently attributes its stability to the shear-flow stabilization mechanism.

MOTIVATION

Investigation into pinch-based plasma physics is an active field of inquiry, and largely has been since the early days of research into the physics and engineering

of plasma reactors for producing energy from the fusion of light atoms. Modern research into this subject is a rich scientific business whose major projects command expensive computer time for simulation and analysis campaigns which must be waged in order to understand the output from the fusion plasma diagnostics attached to the large, high-voltage, high-powered, experimental systems which generate the plasma, and cause the magnetic pinch(es) to occur[8][9].

Alongside this, a theoretical understanding of pinch behavior is naturally required in order to interpret the experimental observations. Modern investigations of this kind center around, and are enriched, both by the presence of nonlinear physics, as well as the subject of plasma turbulence, due to the form that the natural evolution of the pinch plasma frequently takes in experiments. Although the vortical equilibrium plasma flow which is the subject of this research paper is not the same thing, strictly-speaking, as a form of strong or weak MHD turbulence, the notion of vorticity is fundamentally entangled with the study of turbulence[10][11]. Obtaining shear-flow stabilization conditions to a nonlinear, vortical, ideal plasma equilibrium is interesting for a multitude of reasons, both in of itself and as a platform for further work on the science of SFS Z-Pinches.

It is also of particular interest that the current density profile of the Bennett Pinch is the flow state under consideration here. The Bennett Pinch is one of the oldest topics in plasma physics, with perhaps only Langmuir and ionospheric Whistler waves being older. Studying the conditions on this form for shear-flow stabilization in the ideal limit is of interest in general as this limit merely corresponds to the shear being positive definite.

BACKGROUND

Research into fluid dynamics is one of the most active fields of modern physics as it brings together a wide range of scientific discplines, and offers a rich variety of problems to researchers. When the electrical conductivity of the fluid is considered then the finite electric and magnetic fields which exist as a consequence of the flow of electric charge must be incorporated into the governing equations of fluid dynamics, and the range of possible behaviors expands.

In the ideal limit, which can be interpreted as meaning no magnetic diffusivity $\lambda = (\mu\sigma)^{-1}$, or more thoroughly, an infinite magnetic Reynold's number,

$$R_m = \sigma\mu u L \tag{8}$$

then the magnetic field acts as if it were "frozen-in" to the plasma, meaning that it is transported along with the plasma flow. The basic mechanism behind this arises from nature's abhorrence for a change in the magnetic flux of a system. Consequently, an equilibrium MHD plasma can be treated as a magnetic spring, because, in the absence of magnetic diffusion the only dynamics which are observable are the ones induced by a displacement from the magnetic equilibrium according to Lenz's law. In other words, to keep the magnetic flux the same, any arbitrary change in the field at any point in the plasma will arbitrarily induce currents in the plasma volume of such a form so as to counteract this change via their self-generated magnetic fields.

Ideal Magnetohydrodynamics

Ideal MHD, which is of course the aforementioned ideal limit to magnetohydrodynamics and hereafter referred to just as MHD for the rest of the scope of this paper, is the simplest form that a system of governing equations for the behavior of an electrically-conducting fluid can meaningfully take. A "first-principles" derivation of this system, starting from taking suitably-closed moments of kinetic equations describing the evolution of one-particle distribution functions for each plasma species in a full 6D+t phasespace, before appropriately reducing the resulting set of fluid equations to the ideal limit, is outside the scope of this article.

Instead, a satisfactory expression for the homogeneous form of the system is provided below for when there are no inhomogeneities present, e.g., collisions, external sources of mass, momentum, or energy, etc.. The ideal gas law which is commonly used to close the moment-taking process is included at the end, and note that in Equation (15) the electrons are assumed to carry the current, with immobile ions,

$$\frac{\partial \rho}{\partial t} + \nabla \cdot (\rho \vec{u}) = 0 \tag{9}$$

$$\frac{\partial \rho \vec{u}}{\partial t} + \nabla \cdot (\rho \vec{u}\vec{u} - \frac{\vec{B}\vec{B}}{\mu_0} + (p + \frac{B^2}{2\mu_0})\underline{\underline{I}}) = 0 \tag{10}$$

$$\frac{\partial \vec{B}}{\partial t} + \nabla \cdot (\vec{u}\vec{B} - \vec{B}\vec{u}) = 0 \tag{11}$$

$$\frac{\partial e}{\partial t} + \nabla \cdot ((e + p + \frac{B^2}{2\mu_0})\vec{u} - \frac{\vec{B} \cdot \vec{u}}{\mu_0}\vec{B}) = 0 \tag{12}$$

$$\rho \simeq m_i n \tag{13}$$

$$e = \frac{p}{\gamma - 1} + \frac{\rho \vec{u} \cdot \vec{u}}{2} + \frac{B^2}{2\mu_0} \tag{14}$$

$$\vec{J} = -ne\vec{u} \tag{15}$$

$$\vec{E} = -\vec{u} \times \vec{B} \tag{16}$$

$$p = 2nk_B T \tag{17}$$

The above system of eight nonlinear, hyperbolic, partial differential equations expresses the evolution of mass, momentum, energy, and magnetic field in a flat spacetime, at non-relativistic speeds, and they are coupled to relations for the current density, electric field, plasma pressure, plasma mass density, and internal energy. Together Equations (9) - (17) completely describe the ideal behavior of a fluid plasma in arbitrary geometry.

Axisymmetric MHD Equilibrium

When a homogeneous MHD flow is steady, meaning it features no quantities which depend on time, then the governing equations simplify, and they now express strong conditions for there being no divergence of the flux associated with any conservative MHD variable. Additionally, if the flow is cylindrical, and axisymmetric, meaning in the context of a cylindrical flow that its properties depend only on the radial coordinate, then it possesses both an axial, and azimuthal symmetry, and the equations simplify even further because all the axial and azimuthal derivatives vanish from the equations.

Ordinarily, the bulk plasma flow is taken to be static, i.e., $\vec{u} = 0$, or uniform, $\vec{u} = u_0\hat{u}$, in order to simplify the LHS of the momentum equation so that the force balance rests entirely on the Lorentz force and plasma pressure gradient. When the bulk plasma flow is instead nonuniform, then the equilibrium is that of a dynamic one, and there are three equations which largely define dynamic, cylindrical, axisymmetric MHD equilibria[12],

$$\nabla \cdot \vec{B} = 0 \tag{18}$$

$$\nabla \times \vec{B} = \mu_0 \vec{J} \tag{19}$$

$$\rho\vec{u} \cdot \nabla\vec{u} = \vec{J} \times \vec{B} - \nabla p \tag{20}$$

with the difference in general between the dynamic and the static case being contained in the convective term that now shows up on the LHS of Equation (20). This term vanishes if the plasma flow is uniform, of a perturbative amplitude, or in certain equilibrium cases, e.g., a flowing Z-pinch[13]. Then it becomes,

$$\frac{\mathrm{d}p}{\mathrm{d}r} = -J_z B_\theta \tag{21}$$

Z-Pinch

The Z-pinch is the simplest possible axisymmetric configuration for magnetically confining a plasma whereby the Lorentz force of an axial plasma current, and the associated azimuthal magnetic field compresses ("pinches") the plasma inward against the outward-directed plasma pressure gradient,

$$\vec{J} = J_z(r)\hat{z} \tag{22}$$

$$\vec{B} = B_\theta(r)\hat{\theta} \tag{23}$$

$$\nabla p \to \frac{\mathrm{d}p}{\mathrm{d}r}\hat{r} \tag{24}$$

according to Equation (20). Note that the LHS of this equation, i.e., the convective non-linearity term, will be identically zero for an arbitrary Z-pinch equilibrium because the radial transport of momentum due to the advection of flow gradients through the pinch goes to zero. In general, this term reads,

$$(\vec{u} \cdot \nabla\vec{u})_r = u_r\frac{\partial u_r}{\partial r} + \frac{u_\theta}{r}\frac{\partial u_r}{\partial \theta} + u_z\frac{\partial u_r}{\partial z} - \frac{u_\theta^2}{r} \tag{25}$$

from the above it is obvious why this term will be 0 for an axisymmetric Z-pinch.

When fusion research was first declassified internationally in the 50s researchers believed, largely on the back of the Z-pinch's simplicity, and buoyed by the rousing success of controlling fission, that igniting a Z-pinch would be a simple task. However, this was not the case as the Z-pinch suffers from $m = 0$, and $m = 1$ MHD instabilities, as can be shown via normal-mode analysis or an energy principle, as well as large parallel heat (end) losses, and the device was largely abandoned as a reactor concept because it was determined to be impossible to generate a fusing Z-pinch which lived long enough to break-even.

Still, the Z-Pinch remains the most promising magnetic confinement fusion (MCF) configuration because of its lack of need for external magnets, small form-factor, and unity beta[3] which makes it the simplest, and most cost-advantageous device, from an engineering perspective, when compared to toroidal configurations like the tokamak, or stellarator. In addition to their large form factor, and expensive external components, tokamaks also suffer from disruptions caused by runaway electrons. This last part is a serious problem for a "backbone reactor", meaning one which serves to provide base-band power for a modern energy grid, as it will either require the storage of sufficient electrical energy to maintain grid operation during disruptions, or multiple tokamaks would be required in a node, thereby further increasing the cost, and complexity of the plant.

Shear-Flow Stabilization

Modern Z-pinch fusion science also benefits from joinder with a stabilized form of the Z-pinch based on shear-flow-driven phase mixing of the different instabilities that allows a pinch lifetime which exhibits gross stability for many Alfven transit times[14]. Previous successful attempts to stabilize the Z-pinch involved the usage of wall image currents, hard-cores, or external arrays of magnetic coils to produce a stable confinement. None of these solutions are "power plant friendly" as, respectively, they will either lead to unsustainably short service lifetimes due to the enhanced melting of the wall, increased expense and operational downtime from the need for hard-core procurement and maintenance, and in general just increase the engineering costs, and complexity while presenting a set of new problems which lead the Z-pinch away from what makes it so promising, if stabilized in a manner independent of the aforementioned problematic mechanisms. Which, it has been[5].

The modern, shear-flow stabilized (SFS) Z-Pinch is currently being developed at Zap Energy, and the FuZE device is currently the subject of a number of computational studies which focus on simulating the plasma using multi-fluid models[15]. These studies are closely coupled to theoretical work on the subject, where the leading thought is to model the pinch using the marginally-

stable equilibrium of Kadomtsev[16]. Experimental observations of FuZE show a rotating, turbulent pinch with a lifetime that is on the order of 1,000's of Alfven times, indicating the achievement of a quasi-equilibrium Z-pinch whose base flow possesses a non-uniform character. This magnetic stability arises from a shear flow in the axial plasma velocity of the axisymmetric equilibrium, meaning,

$$\frac{\mathrm{d}u_z}{\mathrm{d}r} > 0.1kV_A \tag{26}$$

where $k = \frac{2\pi}{L}$ is naturally the axial wavenumber of the destabilizing mode, and $V_A = \frac{B}{\sqrt{\rho\mu}}$ is the velocity of Alfven waves, i.e., transverse disturbances in the magnetic field which play a fundamental role in the plasma dynamics of MHD turbulence because they can travel in the direction of a field line while possessing an arbitrary waveform. The above expression can be manipulated into the form,

$$\frac{\mathrm{d}u_z}{\mathrm{d}r} > \sqrt{\frac{\mu}{\rho}}\frac{\pi B\sigma u}{5R_m} \tag{27}$$

Taking the ideal limit, $R_m \to \infty$, we arrive at the ideal condition,

$$\frac{\mathrm{d}u_z}{\mathrm{d}r} > 0 \tag{28}$$

A couple of notes must be made at this junction. Strictly-speaking, the above limit-taking process to reach an ideal situation is not the same thing as reaching that ideal situation via an infinite conductivity, $\lim_{\sigma\to\infty} R_m = \infty$. The latter of course being the situation by which fusion plasma scientists accord ideality to a fusion plasma on the basis of the high temperatures. Instead, the argument for ideal behavior here is based directly on the consideration of an infinitely long plasma column.

Bennett Pinch

Let us consider a Z-pinch where Equation (22) is described by,

$$J_z(r) = \frac{-en_0u_{z,0}}{(1+\xi^2r^2)^2} \tag{29}$$

which is the classic Bennett current, and can be inserted into Ampere's Law, Equation (19), then integrated via u-substitution or symbolic computation to yield the azimuthal magnetic field that provides the magnetic tension,

$$B_\theta(r) = -\frac{A}{2}\frac{r}{(1+\xi^2r^2)} \tag{30}$$

$$A = \mu_0 en_0 u_{z,0} \tag{31}$$

For a classic Bennett Pinch, this is enough to completely solve the entire system as the plasma number density has already been specified. Note that due to the uniform flow velocity this flow possesses identically zero vorticity,

$$\vec{\omega} = \nabla \times \vec{u} \tag{32}$$

and note as well that the magnetic tension is absent any singularities, but also gives a trivial answer for the field in the plasma core. Normalized profiles of these quantities are plotted in Figures (1), (2), and (3).

An analytic form for the plasma pressure of a Bennett Pinch can be integrated from the equation of motion with a suitable choice for the pressure of the core plasma, p_0,

$$p(r) = p_0 - \frac{A^2}{8\mu_0}r^2\frac{2+\xi^2r^2}{(1+\xi^2r^2)^2} \tag{33}$$

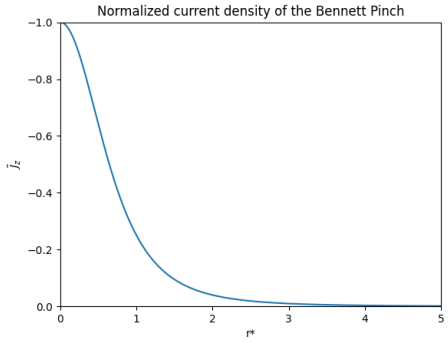

Figure 1. Normalized profile of the plasma current density for a Bennett Pinch, Equation (29). $\tilde{J}_z = \frac{J_z}{en_0u_{z,0}}$, and $r^* = \frac{r}{L^*} = r\xi$. The key feature to notice is the evanescence of the profile over a handful of scale-lengths without the need for any piecewise constructions that introduce discontinuities in the solution.

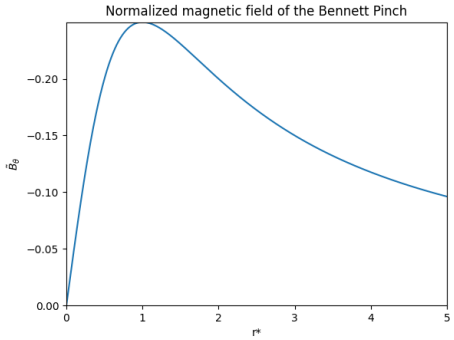

Figure 2. Normalized profile of the magnetic field for a Bennett Pinch, Equation (30), with $\tilde{B}_\theta = \frac{\xi}{A}B_\theta$. Note the need to introduce an extra factor of ξ into the form in order to properly normalize the length, completely. Outside of the region where the bulk plasma current goes to zero the magnetic field goes as $\sim \frac{1}{r}$ while inside this region the shape of the field is influenced by the nonlinear plasma current. Comparison with the other normalized profiles will convince that this $\frac{1}{r}$-dependence is a much slower falloff, comparatively. Also, observe that the theory gives a trivial solution for the value of the core magnetic field.

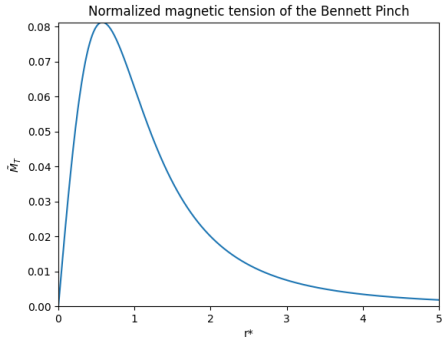

Figure 3. Normalized profile of the magnetic tension for a Bennett Pinch, $M_T = \frac{B_\theta^2}{\mu r}$. The normalized profile displayed here is given by $\tilde{M}_T = M_T \frac{\mu \xi}{A^2} = \frac{\tilde{B}_\theta^2}{r^*}$. The lack of singularity in the profile is due to the nonlinear dependence of B_θ, i.e., the Bennett profile.

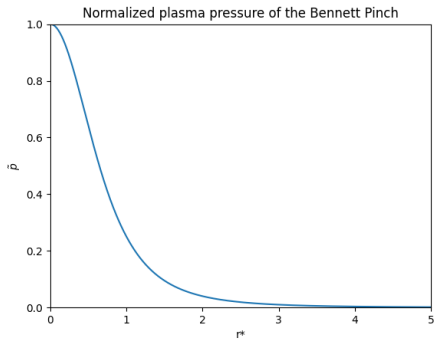

Figure 4. Normalized plasma pressure of the Bennett Pinch as a function of the dimensionless coordinate $r^* = r\xi$. $\tilde{p} = \frac{p}{p_0}$ is plotted here, and there is a specific requirement for $p_0 = \frac{A^2}{8\xi^2\mu}$ to achieve the dimensionless form. This amounts to the trivial constraint that $T \neq 0$ which is an uninteresting limit in the theory because it represents a plasma with zero thermal energy, i.e., a trivial one as far as fusion plasma physics is concerned.

and the profile is plotted in Figure (4). Note that, unlike the Bennett Pinch, an adiabatic gas law cannot be invoked in the case of a Bennett Vortex as it would violate the requirement that a Bennett Vortex has for a uniform density, so an ideal gas law must then be specified to close the system of equations. This translates into a temperature gradient, rather than a density, and consequently the Bennett parameter, $b \to b(r)$, now becomes spatially-dependent since it is directly related to an inverse temperature. This feature is the main difference between a Bennett Vortex and the classic Bennett Pinch equilibrium.

RESULTS

Bennett Vortices

When the plasma flow carries the nonlinearity, instead of the plasma density, the key difference is that the plasma pressure gradient is now supported by a temperature gradient, instead of a density gradient. This fact is extremely relevant in a Bennett Vortex as the Bennett parameter, b, given by Equation (4), now is host to a spatially-dependent temperature which must be dealt with, and introduces significant complexity into the governing equations which must be considered.

The most important consideration is the ideal shear-flow stabilized Z-Pinch criterion,

$$\frac{\mathrm{d}u_z}{\mathrm{d}r} > 0 \tag{34}$$

which can be derived from the general criterion, Equation (26),

$$\begin{aligned} \frac{\mathrm{d}u_z}{\mathrm{d}r} &> 0.1 k V_A \\ &= 0.1\left(\frac{2\pi}{L}\frac{B}{\sqrt{\rho\mu_0}}\right) \\ &= \sqrt{\frac{\mu_0}{\rho}}\frac{\pi B \sigma u}{5 R_m} \end{aligned}$$

in the limit that $R_m \to \infty$, or equivalently here $L \to \infty$, and when the magnetic field is finite. Then the above reduces to Equation (34). Fusion plasmas are predicted to behave as they do because of the high temperatures which imply an infinite conductivity[17], but in practice large accelerating electric fields also means that high-fidelity modelling of fusion plasma dynamics requires the incorporation of relativistic physics as the interesting physics occurs at the tail of the distribution. The higher the temperature of the reaction, then the more important this becomes for open-end configurations like the SFS Z-Pinch. Additionally, the SFS Z-Pinch has the fundamental scientific problem at its core of characterizing the deflagration mode which results from the onset of the thermonuclear reactions[5] which occur amidst the turbulent development of shear-flow stabilization from the seed snowplow.

Beyond potential applications to fusion energy, the idea of Bennett Vortices are also a promising application to very long, coherent, astrophysical structures in regions of steady density. For example, this is a possible mechanism explaining why it is that there are streamers which form (in) the cosmic web. Perhaps with a suitable temperature profile, like that of a core with some parabolic loss to the edge state which jumps to the vacuum, they manage to maintain roughly stable states because they are very long and roughly uniform in density from the perspective of an observer viewing the very long columns of hydrogen plasma from a macroscopic perspective.

From a theoretical perspective it is perfectly valid to do this, but computationally the closest that can be achieved in a numerical investigation is the implementation of periodic axial boundary conditions. These are of course an imperfect representation of an infinite plasma as information from a specific point on the mesh will eventually begin interfering with itself as it flows through the periodic boundary.

In this vein, the shear of a Bennett Vortex is described by,

$$\begin{aligned}\frac{\mathrm{d}u_z}{\mathrm{d}r} &= \frac{\mathrm{d}}{\mathrm{d}r}\left(\frac{u_{z,0}}{(1+\xi^2r^2)^2}\right)\\ &= \frac{-2u_{z,0}}{(1+\xi^2r^2)^3}\left[-r^2n_0\frac{b}{T}\frac{\mathrm{d}T}{\mathrm{d}r}+2\xi^2r\right]\\ &= \frac{2\xi^2ru_{z,0}}{(1+\xi^2r^2)^3}\left[\frac{r}{T}\frac{\mathrm{d}T}{\mathrm{d}r}-2\right] \qquad (35)\end{aligned}$$

and can be considered as being composed of two terms,

$$I = \frac{2\xi^2ru_{z,0}}{(1+\xi^2r^2)^3} \qquad (36)$$

$$II = \frac{r}{T}\frac{\mathrm{d}T}{\mathrm{d}r}-2 \qquad (37)$$

Conformance to the ideal form of the SFS Z-Pinch criterion requires that neither of I and II be zero, and that both either be positive, or negative. It is simplest to first consider the case when $II > 0$ as, assuming that $T(r) = a_nr^n$ this gives the requirement that,

$$\frac{r}{T}\frac{\mathrm{d}T}{\mathrm{d}r} > 2 \qquad (38)$$

$$\rightarrow \frac{r}{a_nr^n}a_nnr^{n-1} > 2 \qquad (39)$$

$$\rightarrow \frac{a_n}{a_n}\frac{r^{n-1}}{r^{n-1}}n > 2 \qquad (40)$$

$$\therefore n > 2 \qquad (41)$$

The simplest temperature profile which fits this bill is,

$$T(r) = C_Tr^3 \qquad (42)$$

naturally leading the coupling constant, C_T, to take the form,

$$C_T = \frac{T(r_p)}{r_p^3} \qquad (43)$$

Then, in general, the expression II becomes,

$$II = \frac{r}{C_Tr^3}C_T3r^2-2 \qquad (44)$$

$$= 3-2 \qquad (45)$$

$$= 1 \qquad (46)$$

which is clearly greater than 0 regardless of the value of the temperature's coupling constant, which carries units of temperature over volume. The expression I, which now represents the whole shear, then becomes,

$$\frac{\mathrm{d}u_z}{\mathrm{d}r} = I = 2\frac{C_B}{C_T}n_0\frac{u_{z,0}}{r^2}\frac{1}{(1+\frac{1}{r}\frac{C_Bn_0}{C_T})^3} \qquad (47)$$

$$= 2C_{B,T}u_{z,0}\frac{r}{(r+C_{B,T})^3} \qquad (48)$$

with,

$$C_{B,T} = \frac{C_B}{C_T}n_0 \qquad (49)$$

Via inspection Equation 48 can be seen to be greater than zero everywhere as all values involved will be positive. At the origin, the shear becomes,

$$\frac{\mathrm{d}u_z}{\mathrm{d}r}|_{(r=0)} = \frac{2u_{z,0}}{C_{B,T}^2} \qquad (50)$$

One loose end which must be addressed before moving onto the finite length theory is the magnetic field. In the limit taken we assumed that the shear threshold went to zero, so now we must check that the magnetic field does not run to infinity.

Ampere's Law governs the relationship between current and magnetic field as stated previously, and for an axisymmetric Z-Pinch it reduces to the ODE,

$$\frac{\mathrm{d}(rB_\theta)}{\mathrm{d}r} = \mu_0rJ_z(r) \qquad (51)$$

where the cubic temperature profile gives,

$$J_z(r) = -en_0u_{z,0}\frac{r^2}{(r+C_{B,T})^2} \qquad (52)$$

so that Ampere's Law becomes, step-by-step,

$$B_\theta = \frac{\mu_0}{r}\int_0^r r'J_z(r')dr' \qquad (53)$$

$$\therefore B_\theta = \frac{-en_0\mu_0u_{z,0}}{r}\int_0^r\frac{r'}{(1+\xi^2(r')r'^2)^2}dr' \qquad (54)$$

with r' representing a dummy variable of integration. Next, we insert $\xi^2 = bn_0 = \frac{n_0C_B}{T(r)}$ into the above, obtaining,

$$B_\theta(r) = \frac{-en_0\mu_0u_{z,0}}{r}\int_0^r\frac{r'}{(1+\frac{C_Bn_0}{T(r')}r'^2)^2}dr' \qquad (55)$$

$$= \frac{-en_0\mu_0u_{z,0}}{r}\int_0^r\frac{T^2(r')r'}{(T(r')+C_Bn_0r'^2)^2}dr' \qquad (56)$$

with $T(r) = C_Tr^3$,

$$B_\theta(r) = -\frac{\mu_0en_0u_{z,0}}{r}\int_0^r\frac{r'^7}{r'^4}\frac{C_T^2}{C_T^2}\frac{1}{(r+C_{B,T})^2}dr' \qquad (57)$$

$$= -\frac{\mu_0en_0u_{z,0}}{r}\int_0^r\frac{r'^3}{(r'+C_{B,T})^2}dr' \qquad (58)$$

this integral can be evaluated with the aid of the Computer Algebra Software (CAS), Wolfram Mathematica,

$$\int_0^r \frac{r'^3}{(r'+C_{B,T})^2}dr' = \frac{f(r,C_{B,T})}{2(r+C_{B,T})} \tag{59}$$

where,

$$f(r,C_{B,T}) = f_1 + f_2 + f_3 + f_4 \tag{60}$$

with,

$$f_1(r) = r^3 \tag{61}$$
$$f_2(r,C_{B,T}) = -3r^2C_{B,T} \tag{62}$$
$$f_3(r,C_{B,T}) = -6rC_{B,T}^2(1+\ln\left(\frac{C_{B,T}}{r+C_{B,T}}\right)) \tag{63}$$
$$f_4(r,C_{B,T}) = -6C_{B,T}^3\ln\left(\frac{C_{B,T}}{r+C_{B,T}}\right) \tag{64}$$

yielding,

$$\vec{B} = B_\theta(r)\hat{\theta} = -\frac{\mu_0 e n_0 u_{z,0}}{2r(r+C_{B,T})}f(r,C_{B,T})\hat{\theta} \tag{65}$$

The Mathematica notebooks which support the above result can be found here.

A plot of the normalized flow, and flow-shear, profiles for an r^3 Bennett Vortex is shown in Figure (5) and Figure (6), respectively. The normalized flow profile has the form,

$$u_z(r) = \frac{u_{z,0}}{(1+\xi^2r^2)^2} \tag{66}$$
$$= \frac{u_{z,0}}{(1+\frac{C_{B,T}}{r})^2} \tag{67}$$
$$= u_{z,0}\frac{r^2}{(r+C_{B,T})^2} \tag{68}$$
$$= \frac{u_{z,0}}{C_{B,T}^2}\frac{r^2}{(\phi+1)^2} \tag{69}$$
$$= \frac{u_{z,0}}{C_{B,T}^2}\frac{(C_{B,T}\phi)^2}{(\phi+1)^2} \tag{70}$$
$$= u_{z,0}\frac{\phi^2}{(\phi+1)^2} \tag{71}$$

$$\therefore \tilde{u}_z = \frac{\phi^2}{(\phi+1)^2} \tag{72}$$

$$\rightarrow \frac{\mathrm{d}\tilde{u}_z}{\mathrm{d}\phi} = \frac{2\phi}{(\phi+1)^2} - 2\frac{\phi^2}{(\phi+1)^3} \tag{73}$$

The remaining equilibrium quantity to address is the plasma pressure. In general for a Bennett Vortex the momentum balance leads to the equation,

$$\frac{\mathrm{d}T}{\mathrm{d}r} = -\frac{(en_0u_{z,0})^2\mu_0}{2n_0k_Br}\frac{T(r)^2}{(T+C_Bn_0r^2)^2}\int_0^r \frac{r'T(r')^2}{(T+C_Bn_0r^2)^2}dr'$$

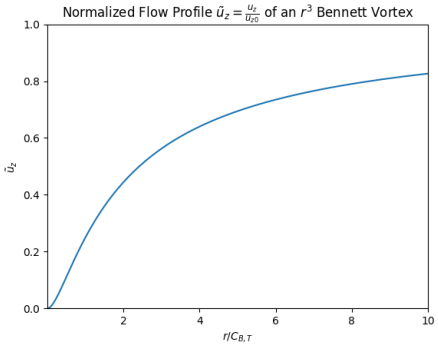

Figure 5. The normalized flow profile of an r^3 Bennett Vortex. The asymptotic behavior of the normalized flow profile is to tend to unity, representing the edge flow state, as the dimensionless coordinate, ϕ goes to ∞. For values of $\phi < 1$ the flow profile has an approximately parabolic character that changes to more of a logarithmic appearance as the point of maximal shear is reached, which is intriguingly similar to the axial velocity profiles seen in the ZaP[14] and FuZE machines.

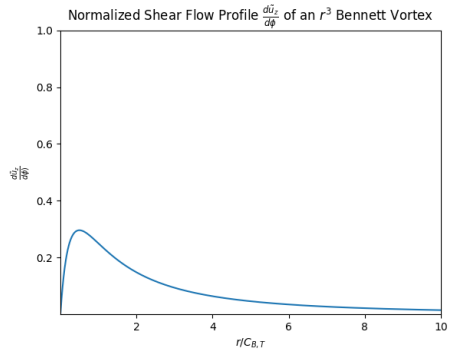

Figure 6. The normalized flow-shear of an r^3 Bennett Vortex. The maximum shear occurs at $\phi = \frac{1}{2}$, and the asymptotic behavior of the shear is to go to zero at $r \rightarrow \infty$ as can be seen from the graph, or from analyzing Equation (73).

which is a substantially challenging integral, however, from our analysis of the ideal limit of this MHD equilibrium we see that it is suggestive of trying a temperature of order $n > 2$.

For an r^3 Bennett Vortex, where the magnetic field is tractable, if we assume that the pressure follows an ideal gas law then we have instead,

$$\frac{12n_0k_BT_p}{\mu_0(en_0u_{z,0})^2r_p^3}r(r+C_{B,T})^3 + f = 0 \tag{74}$$

which is a fourth-order polynomial whose roots describe the points in the plasma where the plasma pressure is the same as the ideal gas pressure. This can be derived from the momentum balance, Equation (21) for this flavor of

Bennett Vortex,

$$\begin{aligned}
&\frac{\mathrm{d}p}{\mathrm{d}r} = -J_z B_\theta \\
\therefore\quad & 6n_0 k_B C_T r^2 + J_z B_\theta = 0 \\
\rightarrow\quad & \frac{6n_0 k_B T_p}{r_p^3} r^2 + \frac{\mu_0 (e n_0 u_{z,0})^2}{2(r + C_{B,T})^2} r \int_0^r \frac{r'^3}{(r' + C_{B,T})^2} dr' = 0 \\
\rightarrow\quad & \frac{6n_0 k_B T_p}{r_p^3} r + \frac{\mu_0 (e n_0 u_{z,0})^2}{2(r + C_{B,T})^3} f = 0 \\
\therefore\quad & \frac{12 n_0 k_B T_p}{\mu_0 (e n_0 u_{z,0})^2 r_p^3} r (r + C_{B,T})^3 + f = 0
\end{aligned}$$

In general, the plasma pressure of a Bennett Vortex should be obtained from integrating the force balance as the ideal gas law is an *ad hoc* closure relation which cedes ground to conservation of momentum, as the latter is a consequence of Noether's Theorem. Continuing in this vein,

$$\begin{aligned}
p(r) &= p_0 - \int_0^r J_z(r') B_\theta(r') dr' \\
&= p_0 - \int_0^r \frac{\mu_0 (e n_0 u_{z,0})^2}{r'(1 + \xi^2 r'^2)^2} \left(\int_0^{r'} r'' \frac{1}{(1 + \xi^2 r''^2)^2} dr'' \right) dr' \\
&= p_0 - \mu_0 (e n_0 u_{z,0})^2 \dots \\
&\qquad \dots \int_0^r \frac{r'}{(r' + C_{B,T})^2} \left(\int_0^{r'} \frac{r''^3}{(r'' + C_{B,T})^2} dr'' \right) dr' \\
&= p_0 - \mu_0 (e n_0 u_{z,0})^2 \int_0^r \frac{r'}{2(r' + C_{B,T})^3} f(r', C_{B,T}) dr'
\end{aligned}$$

This integral can be evaluated with Mathematica. The notebook which facilitated this research can be found here. The pressure turns out to also be tractable, yielding,

$$\begin{aligned}
p(r) = p_0 - \frac{\mu_0 (e n_0 u_{z,0})^2}{4(r + C_{B,T})^2} \Big[& r^4 - 10 r^3 C_{B,T} + \dots \\
& + 3 r^2 C_{B,T}^2 \Big(-13 + 2\ln^2(C_{B,T}) + 6\ln(r + C_{B,T}) \\
& + 2\ln^2(r + C_{B,T}) - 2\ln(C_{B,T})(3 + 2\ln(r + C_{B,T})) \Big) \\
& + 6 r C_{B,T}^3 \Big(-5 + 2\ln^2(C_{B,T}) + 8\ln(r + C_{B,T}) \\
& + 2\ln^2(r + C_{B,T}) - 4\ln(C_{B,T})(2 + \ln(r + C_{B,T})) \Big) \\
& + 6 C_{B,T}^4 \Big(\ln^2(C_{B,T}) + \ln(r + C_{B,T})(5 \\
& + \ln(r + C_{B,T})) - \ln(C_{B,T})(5 + 2\ln(r + C_{B,T})) \Big) \Big]
\end{aligned}$$

For FuZE-like conditions,

$$\begin{aligned}
C_{B,T} &= \frac{C_B n_0}{T_p} r_p^3 \\
&= \frac{\mu_0 e^2 u_{z,0}^2 n_0}{16 k_B} \frac{r_p^3}{T_p} \\
&= \frac{4\pi * 10^{-7} * (1.6 * 10^{-19})^2 (10^4)^2 10^{23}}{16 * 1.38 * 10^{-23}} \frac{(0.3 * 10^{-2})^3}{(1.1604 * 10^7)} \\
&= 1.2558 * 10^{-7} [m]
\end{aligned}$$

is small enough that we can reasonably simplify the computed pressure by neglecting all terms attached to powers of $C_{B,T}$ that are second-order or higher. Doing so obtains,

$$p(r) \approx p_0 - \frac{\mu_0 (e n_0 u_{z,0})^2}{4 C_{B,T}^2} \frac{1}{(\phi + 1)^2} \left(C_{B,T}^4 \phi^4 - 10 \phi^3 C_{B,T}^4 \right) \tag{75}$$

which can be worked into the dimensionless form,

$$\tilde{p}(\phi) = \tilde{p}_0 - \frac{\phi^3}{(\phi + 1)^2} (\phi - 10) + \mathcal{O}(C_{B,T}^2) \tag{76}$$

where,

$$\tilde{p}_0 = \frac{4}{(e n_0 u_{z,0})^2 \mu_0 C_{B,T}^2} p_0 \tag{77}$$

The bundle of constants in the above denominator can be verified to give units of $[N m^{-2}]$ as they should.

The normalized magnetic field can be readily obtained, and algebraic working of Equation (65) will yield,

$$\begin{aligned}
\tilde{B}_\theta(r) &= \frac{B_\theta(r)}{\mu_0 e n_0 u_{z,0} C_{B,T}} \\
&= \frac{1}{2\phi(\phi + 1)} \Big[\phi^3 - 3\phi^2 - 6\phi + 6\phi \ln(1 + \phi) \\
&\qquad + 6\ln(\phi + 1) \Big]
\end{aligned}$$

This is plotted logarithmically in Figure (7), and linearly in Figure (8), The last profile to examine in a normalized context is the pressure profile which is given by Equation (77) to second-order. The full pressure relationship cannot be fully normalized as there are $C_{B,T}$-terms of first and second-order which cannot be disentangled from the expression,

$$\begin{aligned}
\tilde{p}(\phi) = \tilde{p}_0 + \frac{1}{(\phi + 1)^2} \Big[& \phi^4 - 10\phi^3 + 6\phi^4 C_{B,T}^2 + 18\phi^3 C_{B,T} \\
& - 39\phi^2 + 12\phi^3 C_{B,T}^2 + 48\phi^2 C_{B,T} \\
& - 30\phi + 6\phi^2 C_{B,T}^2 + 30\phi C_{B,T} \Big]
\end{aligned}$$

therefore either this form may be computed directly for a given plasma state, or an approximate form may be derived based on the smallness of $C_{B,T}$.

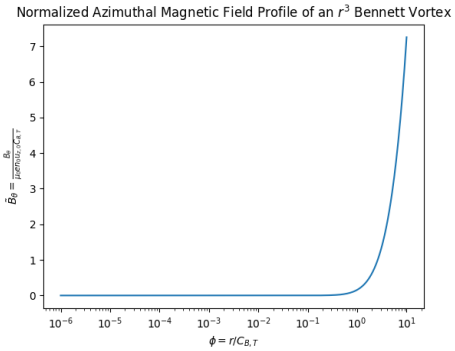

Figure 7. Logarithmic view of the normalized azimuthal field of an r^3 Bennett Vortex. This logarithmic view illustrates that the structure of the field possesses both a magnetic null at the axis, as is seen more clearly in a linear graph, and an extremum point at the pinch radius as this is the largest radius for which the field is valid.

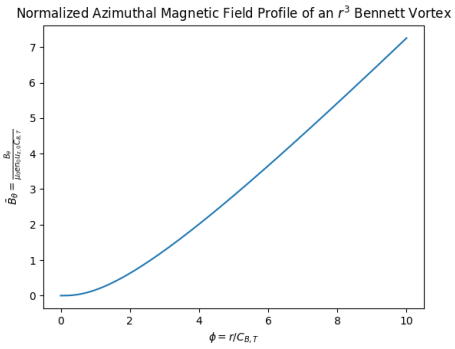

Figure 8. Linear view of the normalized azimuthal field of an r^3 Bennett Vortex. This linear view illustrates clearly that the structure of the field possesses both a magnetic null at the axis, as well as an extremum point at the pinch radius given that this is the largest radius for which the field is valid.

Let us also compute the enclosed current in the r^3 Bennett Vortex SFS device,

$$I_{encl} = \int_0^{2\pi} \int_0^{r_p} r J_z(r) dr d\theta$$

$$\begin{aligned} \therefore I_{encl} = \frac{2\pi e n_0 u_{z,0}}{2(r_p + C_{B,T})} \Bigg[& r_p^3 - 3r_p^2 C_{B,T} \\ & - 6 r_p C_{B,T}^2 (1 + \ln\left(\frac{C_{B,T}}{r_p + C_{B,T}}\right)) \\ & - 6 C_{B,T}^3 \ln\left(\frac{C_{B,T}}{r_p + C_{B,T}}\right) \Bigg] \end{aligned}$$

which can be seen to have units of Amperes. This form can be normalized,

$$\begin{aligned} \tilde{I}_{encl} &= \frac{I_{encl}}{\pi e n_0 u_{z,0} C_{B,T}^2} \\ &= \frac{1}{\phi_p + 1} \Big[\phi_p^3 - 3\phi_p^2 - 6\phi_p \\ &\quad + 6\phi_p \ln(\phi_p + 1) + 6 \ln(\phi_p + 1) \Big] \end{aligned}$$

A plot of this normalized profile is shown in Figure (9)

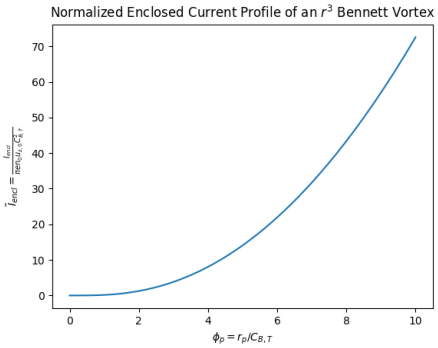

Figure 9. The normalized enclosed current profile, $\tilde{I}_{encl}$ of an r^3 Bennett Vortex.

Mixed Cubic Vortices

Because the cubic, pure-flow, vortex has an analytic equilibrium then so too does any distribution of the Bennett nonlinearity which leaves the cubic, pure-flow vortex current remaining,

$$n(r) = \frac{n_0}{(1 + \xi^2 r^2)^\nu} \tag{78}$$

$$u_z(r) = \frac{u_{z,0}}{(1 + \xi^2 r^2)^\chi} \tag{79}$$

which demands that

$$\nu + \chi = 2 \tag{80}$$

in order to obtain the cubic, pure-flow, $\chi = 2$, vortex current given in Equation (82). A full exploration of this mixed setting is of course beyond the scope of this work, but it is worth studying some of the characteristics of the "uniform", $\chi = \nu = 1$ case in order to later fit them to predictions from SFS experiments.

Base-flow, $\chi = 2$, Cubic Vortices

It is also possible to append an offset to the cubic flow without changing the shear of the vortices. Consider the

pure-flow ($\chi = 2$) cubic vortex flow,

$$u_z(r) = u_0 + u_{z,0}\frac{r^2}{(r + C_{B,T})^2} \tag{81}$$

$$\rightarrow J_z(r) = -en_0\left(u_0 + u_{z,0}\frac{r^2}{(r + C_{B,T})^2}\right) \tag{82}$$

which allows the magnetic field to be integrated,

$$B_\theta = -en_0\mu_0\left(u_0\frac{r}{2} + u_{z,0}\frac{1}{2r(r + C_{B,T})}f(r, C_{B,T})\right) \tag{83}$$

the momentum equation then becomes,

$$\frac{\mathrm{d}p}{\mathrm{d}r} = -J_z B_\theta \tag{84}$$

$$= -\mu_0 e^2 n_0^2\left(u_0 + u_{z,0}\frac{r^2}{(r + C_{B,T})^2}\right) \tag{85}$$

$$\left(\frac{u_0}{2}r + u_{z,0}\frac{f(r, C_{B,T})}{2r(r + C_{B,T})}\right) \tag{86}$$

and the plasma pressure,

$$p(r) - p_0 = -\mu_0 e^2 n_0^2\left(P_1 + P_2 + P_3 + P_4\right) \tag{87}$$

$$P_1 = \int_0^r \frac{u_0^2}{2}r'dr' \tag{88}$$

$$P_2 = \int_0^r u_0 u_{z,0}\frac{f(r', C_{B,T})}{2r'(r' + C_{B,T})}dr' \tag{89}$$

$$P_3 = \int_0^r u_0 u_{z,0}\frac{r'^3}{2(r' + C_{B,T})^2}dr' \tag{90}$$

$$P_4 = \int_0^r \frac{u_{z,0}^2}{2}\frac{r' f(r', C_{B,T})}{(r' + C_{B,T})^3}dr' \tag{91}$$

each of these integrals has an analytic solution, but the P_2, and P_4 integrals are truly formidable expressions whose complete forms are given in Appendix A.

Experimental Comparison

Physical theories need to make predictions based on their calculated consequences, and then compare these to real-world experiments. The Python codes which perform these calculations are found here.

Figures (10) and (11) show the predicted axial flow velocity for an r^3 Bennett Vortex under FuZE-like conditions, which are described in the captions. As noted in the captions of the figures, while the scale and values are not exactly correct, the shape of the profile is intriguingly similar to the axial velocity of a real SFS plasma. It also takes the shape of a sigmoid which can be seen by picking a suitably large view of the signal. This discrepancy in the scale and accuracy, as well as the

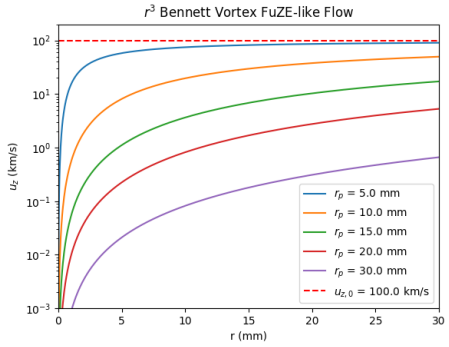

Figure 10. Logarithmic view of the flow profile of an r^3 Bennett Vortex for FuZE-like conditions as it varies with pinch radius according to $r_p = [5, 10, 15, 20, 30]$ [mm]. $u_{z,0} = 100$ $km\ s^{-1}$ is the edge plasma flow state, $T_p = 1$ [keV] is the edge plasma temperature, and $n_0 = 10^{23}$ $[m^{-3}]$ is the plasma number density.

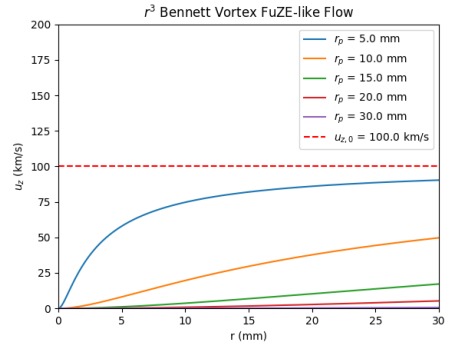

Figure 11. The flow profile of an r^3 Bennett Vortex for FuZE-like conditions as it varies with pinch radius according to $r_p = [5, 10, 15, 20, 30]$ [mm]. $u_{z,0} = 100$ $km\ s^{-1}$ is the edge plasma flow state, $T_p = 1$ [keV] is the edge plasma temperature, and $n_0 = 10^{23}$ $[m^{-3}]$ is the plasma number density. Observe that as pinch radius increases the shear evidently decreases.

appearance of multiple such of these profiles in the case of the $\tau = 0.16$ pulse, can be explained as being due to the intrinsic physics which is not modelled by the homogeneous magnetohydrodynamic theory of an r^3 Bennett Vortex. Namely, the kinetic and relativistic effects which are relevant in a real SFS Z-pinch, as well as the energy of the fusion alphas from the uniform line source. Also, Bennett Vortices are defined in terms of the edge plasma temperature if they are taken as a strict power of the radius given that the predicted core temperature is then absolute zero, which is another interesting wrinkle, and one that further illustrates the importance of kinetic studies.

The importance of these further studies into the kinetics, and relativistic physics of the deflagration process are illustrated in Figures (12), and (13) which show pure-flow cubic vortex states that have been fit to the experimental axial velocity profile of Zap 2001. Figure (14) shows

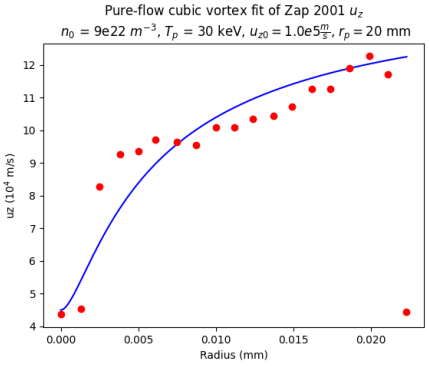

Figure 12. A fit of the pure-flow ($\chi = 2$) cubic vortex flow profile to the axial velocity profile from the 2001 Zap run. Note that the pinch radius, $r_p = 20$ $[mm]$ behind this cubic vortex is taken to be twice the published value. Note as well that the temperature used in the computation of this fit profile is $T_p = 30$ [keV], which is 150x the plasma temperature of the experimental plasma, and also the need for a small $C_{B,T}$ description to avoid solving for the constant $u_{z,0}$. This difference can be explained by the heating of the fusion alphas which occurred in the real SFS plasma. Also note that a base-flow of $u_0 = 45$ $[\frac{km}{s}]$ was employed to fit the profile which is attributed to the establishment of an edge state by the deflagration mode of the fusion reactions. The RRMSE is 20.56%.

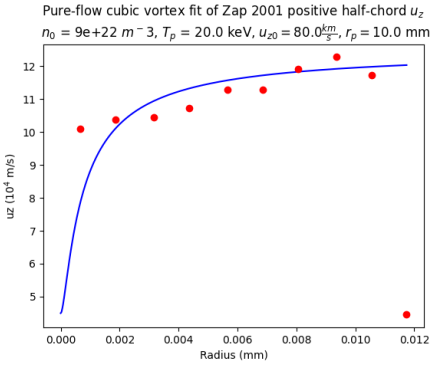

Figure 13. A fit of the pure-flow ($\chi = 2$) cubic vortex profile to the axial velocity profile from the positive half-chord of the 2001 Zap run. The RRMSE is 24.14% with a base-flow of $u_0 = 45$ kms^{-1}.

the flow shear of the FuZE-like, r^3 Bennett Vortex. The predicted azimuthal magnetic field of a FuZE-like experiment for different pinch radii is graphed in Figure (15), Lastly, both linear, logarithmic, and log-log views of the predicted pressure drop of a FuZE-like experiment for different pinch radii are graphed in Figures (16), (17), and (18), respectively, As can be seen from the pressure drop, there are a substantial collection of natural logarithms in the expression, and as can be seen from the pressure drop profiles, these lead to substantial numerical oscillation for small enough values of the radius, although they disappear quickly enough that the form of the pressure drop profile is resolved on macroscopic scales. This calculation

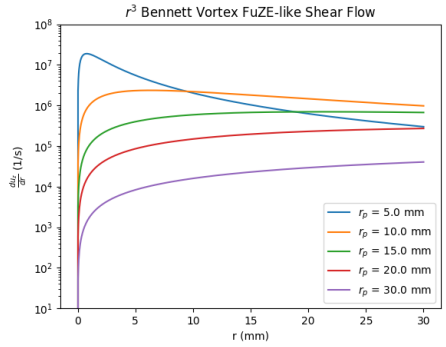

Figure 14. The flow shear of an r^3, FuZE-like Bennett Vortex. The conditions for the calculation are identical to those in Figures (10) and (11). Note the close agreement between the predicted peak flow shear at $r_p = 10$ mm of $\frac{\mathrm{d}u_z}{\mathrm{d}r}_{peak} \simeq 2.36 \times 10^6$ $[s^{-1}]$ and the experimentally observed flow shears varying between $(0-4) \times 10^6$ s^{-1} which is seen in the ZaP flowing Z-Pinch experiments[14]. This suggests that Bennett Vortices form frequently in the ZaP device as the Bennett Vortex flow shear grows quickly in space.

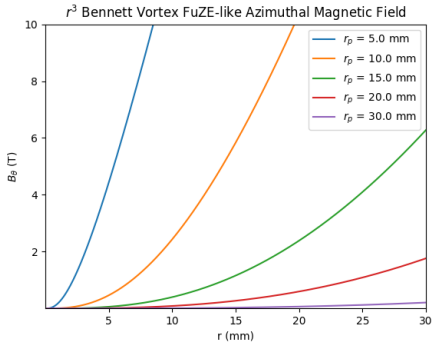

Figure 15. The azimuthal magnetic field predicted for an r^3 Bennett Vortex based on the aforementioned FuZE-like conditions. These predictions are invalid outside of the pinch radius, and also underestimate the magnetic field that is seen at the edge, but they capture the observed features that the magnetic null is at the pinch axis, and that the extremum point is located at the pinch radius.

is invalid outside of the given pinch radius, but for small pinch radii it can be seen to give predictions accurate to the order of magnitude seen in SFS experiments.

We can also plot the enclosed current that an r^3 Bennett Vortex is predicted to have for FuZE-like conditions in Figure (19). The last thing to say in this vein is to study the smallness of $C_{B,T}$ for the conditions of a modern reactor. The smallness of $C_{B,T}$ is critical to the theory because, for example, consider the edge plasma flow of a cubic vortex,

$$u_{edge} = u_z(r_p) = u_{z,0}\frac{r_p^2}{(r_p + C_{B,T})^2} \tag{92}$$

when $C_{B,T}$ is small then these two quantities are approx-

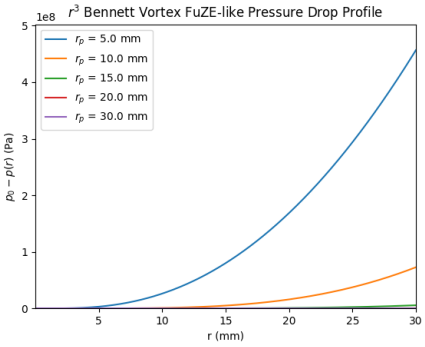

Figure 16. The pressure drop profile for an r^3 Bennett Vortex based on the aforementioned FuZE-like conditions. These predictions are invalid outside of the given pinch radius, and the linear view makes it difficult to resolve the structure of the pressure drop as the pinch radius increases. However, for small values of pinch radius, the predictions of the core plasma pressure agree with experiment up to the order of magnitude.

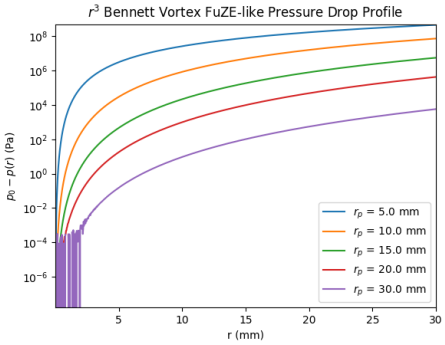

Figure 17. Logarithmic view of the pressure drop profile for an r^3 Bennett Vortex based on the aforementioned FuZE-like conditions. These predictions are invalid outside of the given pinch radius, and the logarithmic view presents numerical oscillations for small values of r due to the natural logarithms in the full expression. However, for small values of pinch radius the predictions of the core plasma pressure agree with SFS experiments up to the order of magnitude.

imately the same. Small-$C_{B,T}$ vortices allow the complicated analytic expressions for pressure and magnetic field to be simplified greatly. Contour plots showing the value of $C_{B,T}$ across a range of conditions characteristic of modern SFS DD fusion experiments are shown in Figures (20), (21), (22), (23), and (24), these figures show that for small pinch radii the small $C_{B,T}$ approximation has a large span of relevant operating conditions over which it is valid.

When $C_{B,T}$ is not small, then $u_{z,0} \neq u_{edge}$. Conse-

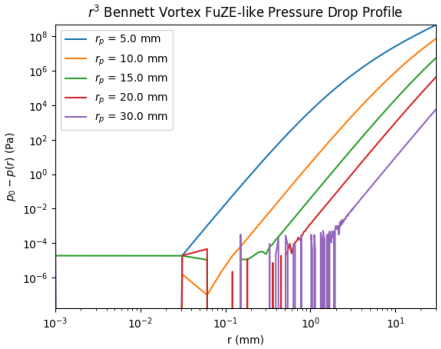

Figure 18. Log-log view of the pressure drop profile for an r^3 Bennett Vortex based on FuZE-like conditions. These predictions are invalid outside of the given pinch radius, and this log-log view presents a fuller picture of the numerical oscillations in the computation for small values of r which are present due to the need to compute natural logarithms in the full expression. However, for small values of pinch radius, the predictions agree with SFS experiments up to the order of magnitude.

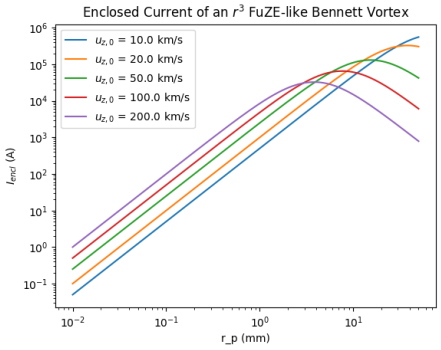

Figure 19. The predicted enclosed current for an r^3 Bennett Vortex in FuZE-like conditions, across a range of edge plasma flow speeds. The order of magnitude seen in experimental results is again reached.

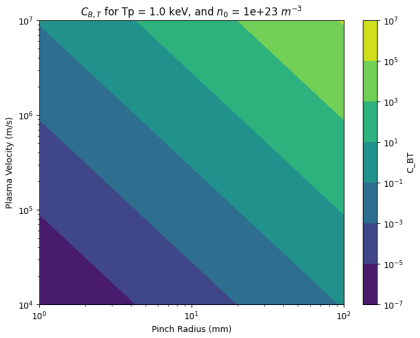

Figure 20. Log-log contour plot of $C_{B,T}$ for a FuZE-like cubic vortex with an edge plasma temperature of $T = 1$ [keV].

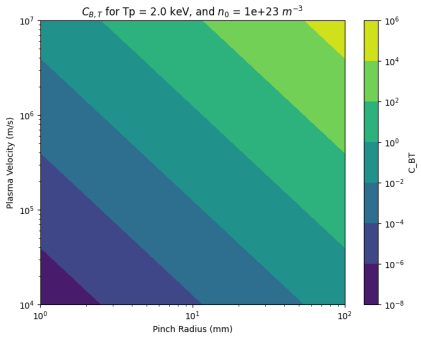

Figure 21. Log-log contour plot of $C_{B,T}$ for a FuZE-like cubic vortex with an edge plasma temperature of $T = 2$ [keV].

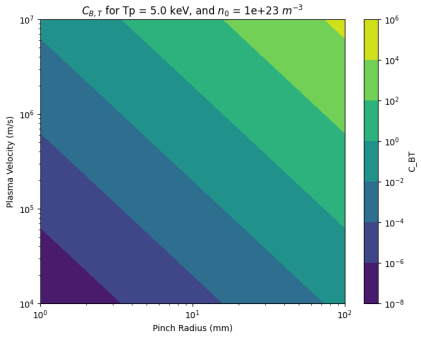

Figure 22. Log-log contour plot of $C_{B,T}$ for a FuZE-like cubic vortex with an edge plasma temperature of $T = 5$ [keV].

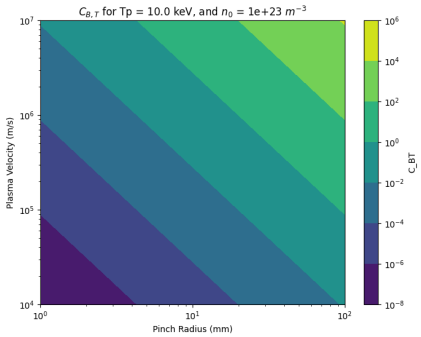

Figure 23. Log-log contour plot of $C_{B,T}$ for a FuZE-like cubic vortex with an edge plasma temperature of $T = 10$ [keV].

quentially, for a pure-flow vortex,

$$u_z(r_p) = u_{edge} = \frac{u_{z,0} r_p^2}{(r_p + C_{B,T})^2} \tag{93}$$

$$\rightarrow u_{z,0} r_p^2 = u_{edge}(r_p + C_{B,T})^2 \tag{94}$$

$$\therefore u_{z,0} r_p^2 - u_{edge}(r_p^2 - 2 r_p C_{B,T} + C_{B,T}^2) = 0 \tag{95}$$

This results in a quartic equation,

$$A u_{z,0}^4 + B u_{z,0}^2 + r_p^2 u_{z,0} - u_{edge} r_p^2 = 0 \tag{96}$$

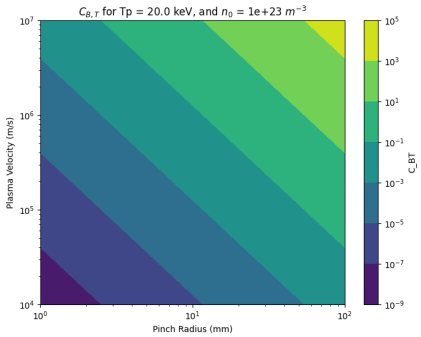

Figure 24. Log-log contour plot of $C_{B,T}$ for a FuZE-like cubic vortex with an edge plasma temperature of $T = 20$ [keV].

where

$$A = \frac{u_{edge} \mu_0^2 e^4 n_0^2 r_p^6}{(16 k_B T_p)^2} \tag{97}$$

$$B = -2 \frac{u_{edge} \mu_0 n_0 e^2 r_p^4}{16 k_B T_p} \tag{98}$$

that can technically be solved as all quartic equations can.

Finite Length Theory

As mentioned previously, the general SFS criterion, 26, is dependent on the longest axial wavelength which the system can bear as this is the fundamental basis on which the parallel transport of magnetic energy necessary to stabilize a Z-Pinch via a shear-flow mechanism is supported. Dealing with the reality of a finite axial length is necessary for fusion applications such as that of a base-band reactor, or electrothermal propulsion, and also for real astrophysical plasmas. Note briefly in the propulsion application that, since a fusion plasma adhering to a Bennett Vortex is predicted to form a pinched cylindrical equilibrium, this would require some stable, and robust means of transferring the impulse to the rocket body. Because fusion plasmas are so hot this medium would either need to be a magnetic field which carries momentum from the ions to the spacecraft body, and/or a liquid metal medium, as a solid thrust plate with contemporary materials would melt. This thrust problem would also require accounting for the inductive electric fields present in the environment due to the exhaust as this exhaust could be highly-ionized if a Bennett Vortex was able to be curtailed into the form of a thruster for a fusion rocket. It is worth seriously considering this equilibrium on these merits alone as a fusion rocket is a silver bullet for any mission within the solar system, such as to go mine asteroids for rare minerals. These missions could be performed with a payload of AI miners, and manned by a crew of specialized human and scientific personnel to oversee the operation. How much mass, representing valuable materials mined from the Asteroid Belt, would be an inappropriate amount to transport back to the Earth is a question to answer, but outside the scope of the current work.

Pure-flow, $\chi = 2$

It is straightforward to insert Eqn 35 into the LHS of the general SFS criterion Equation 26, yielding,

$$\frac{2\xi^2 r u_{z,0}}{(1+\xi^2 r^2)^3}\left[\frac{r}{T}\frac{\mathrm{d}T}{\mathrm{d}r} - 2\right] > 0.1k\frac{B}{\sqrt{\rho\mu_0}} \tag{99}$$

with B being given according to Equation 65, which is valid when $T(r) = C_T r^3$, then we can evaluate both sides of Equation 99 to obtain a condition for the minimum length required to observe an r^3 Bennett Vortex in a plasma column,

$$L > \frac{\pi}{10 C_{B,T} u_{z,0}\sqrt{\rho\mu_0}}\frac{(r+C_{B,T})^3}{r}B_\theta(r) \tag{100}$$

Inserting the r^3 Bennett Vortex magnetic field into this yields,

$$L > \frac{\pi}{20}\frac{\mu_0 e n_0}{\sqrt{\rho\mu_0}C_{B,T}}\frac{(r+C_{B,T})^2}{r^2}f \tag{101}$$

Next, we expand f, and insert it into the previous expression,

$$f(\phi) = C_{B,T}^3\Big(\phi^3 - 3\phi^2 - 6\phi + 6\phi\ln(\phi+1) + 6\ln(\phi+1)\Big)$$

to obtain,

$$L > \frac{\pi e n_0\mu_0}{20\sqrt{\rho\mu_0}}C_{B,T}^2\frac{(\phi+1)^2}{\phi^2}\Big(\phi^3 - 3\phi^2 - 6\phi + 6\phi\ln(\phi+1) + 6\ln(\phi+1)\Big) \tag{102}$$

This can be normalized,

$$\tilde{L} = L * \frac{20\sqrt{\rho\mu_0}}{e\pi n_0\mu_0 C_{B,T}^2} \tag{103}$$

$$> \frac{(\phi+1)^2}{\phi^2}\Big(\phi^3 - 3\phi^2 - 6\phi \tag{104}$$

$$+ 6\phi\ln(\phi+1) + 6\ln(\phi+1)\Big) \tag{105}$$

and plotted against the dimensionless plasma radius, as in Figure(25), as well as having its limits calculated. It is evident from the form of the pure-flow cubic vortex $\tilde{L}(\phi) = \tilde{L}_2(\phi)$ written previously that this will require the application of L'Hopitals rule twice, yielding,

$$\tilde{L}(0) = \frac{1}{2}\lim_{\phi\to 0}\frac{\mathrm{d}^2\tilde{L}_{2,num}}{\mathrm{d}\phi^2} = 0 \tag{106}$$

where the second derivative of the numerator is,

$$\begin{aligned}\frac{\mathrm{d}^2\tilde{L}_{2,num}}{\mathrm{d}\phi^2} = &\\ &(1+\phi)^2\Big(-6+6\phi-\frac{6}{(1+\phi)^2}-\frac{6\phi}{(1+\phi)^2}\\ &\quad+\frac{12}{1+\phi}\Big)\\ &+4(1+\phi)\Big(-6-6\phi+3\phi^2+\frac{6}{1+\phi}+\frac{6\phi}{1+\phi}\\ &\quad+6\log(1+\phi)\Big)\\ &+2\Big(-6\phi-3\phi^2+\phi^3+6\log(1+\phi)\\ &\quad+6\phi\log(1+\phi)\Big)\end{aligned}$$

which can be seen to have a value of zero in the limit of concern. This is an extremely significant result as it implies that arbitrarily close to the pinch axis these vortices can spontaneously form SFS states for arbitrarily small pinch lengths.

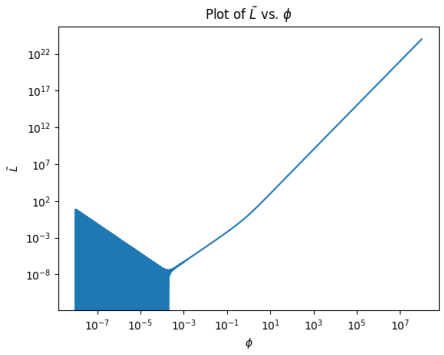

Figure 25. Logarithmic view of the normalized minimum pinch length required for a pure-flow, r^3 vortex to form an SFS Z-Pinch as a function of the dimensionless plasma radius, $\phi = \frac{r}{C_{B,T}}$. The numerical instability present close to the origin is introduced by the computation of the natural logarithms for small values of ϕ. The value of $\tilde{L}(0)$ can be evaluated with L'Hopitals rule.

Uniform flow, $\chi = 1$

Base flow, $\chi = 2$

The biggest discrepancy between the form of the pure-flow, or uniform vortex and the experimental results obtained from real SFS machines is of course in the non-zero core flow that is present in experiments. Therefore, we introduce an offset which leaves the shear unchanged, but changes the structure of the current density, and magnetic field as described in Equations (82), and (83), respectively.

Leaving L, the pinch length out of things, there are four multiscale parameters to evaluate in this equation, namely, $n_0, T(r_p), r_p, u_{z,0}$ which are, respectively, the plasma number density, edge plasma temperature, pinch radius, and edge flow speed. The ranges of interest are shown in Table (I) with the range of pinch lengths included. For an SFS Z-Pinch experiment the range of

Plasma Parameter	Scale	Units
n_0	$10^6 - 10^{30}$	$[m^{-3}]$
L	1	$[m] \sim [parsec]$
T_0	$10^4 - 10^9$	[degK]
r_p	1	$[nm] \sim [psec]$
$u_{z,0}$	1	$[ms^{-1}] \sim [c]$

Table I. Plasma parameter ranges over which Bennett Vortices are of interest. These scales range from astrophysical plasmas, e.g., galaxy filaments which might be stable by virtue of the Bennett Vortex equilibrium, to fusion applications such as MCF baseband, and propulsion, as well as potentially ICF applications, although these would require consideration of smaller pinch lengths than meter-sized.

parameters decreases substantially. It is important to calculate the minimum length required for an r^3 Bennett Vortex to be SFS under these conditions because if it is too long then the SFS character of the equilibrium will be impractical to create or observe. Table (II) lists these parameters. Note that the core plasma temperature in these experiments is taken to be the edge plasma temperature in these calculations with no loss of generality or interpretative problem because the edge of a Bennett Vortex can be located at arbitrary pinch radius. Microscopic r^3 Bennett Vortices could develop inside of a pinching plasma at any point, so it is appropriate to take this temperature to be any value as the axis of the Bennett Vortex could be situated in such a location so as to satisfy this constraint.

Plasma Parameter	Scale	Units
n_0	$10^{23} - 10^{26}$	$[m^{-3}]$
L	1	$[m]$
T_0	$1 - 2$	[keV]
r_p	1 - 50	[mm]
$u_{z,0}$	10 - 200	$[kms^{-1}]$

Table II. Plasma parameter ranges over which contemporary SFS Z-Pinch experiments range.

Figures (26), (27), (28), (29), and (30), show the exact minimum lengths calculated from Equation (102) for FuZE-like plasmas of different pinch radius and edge flow speed. This is done as a function of the dimensionless radial coordinate, ϕ. A unity ϕ implies,

$$\phi = 1 \rightarrow r = C_{B,T} \tag{107}$$

so interpreting these figures requires understanding what the value of $C_{B,T}$ is for these situations. These are readily computed and shown in Figure (31). The dimensionless point at which the plasma is left, i.e., the dimensionless pinch radius, is,

$$\phi_p = \frac{r_p}{C_{B,T}} = \frac{16 k_B T_p}{\mu_0 e^2 n_0 u_{z,0}^2 r_p^2} \tag{108}$$

for each plasma, values outside of this obviously are invalid. As can be seen from the calculated profiles for L_{min}, r^3 Bennett Vortices can be SFS for length scales much shorter than the device length of $L_{experimental} = 50\ [cm]$.

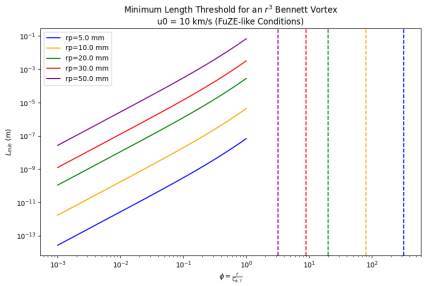

Figure 26. Minimum length required for an r^3 Bennett Vortex to be SFS for FuZE-like conditions with an edge flow speed of $u_{z,0} = 10$ $[km\ s^{-1}]$. Each colored vertical line is the corresponding location of ϕ_p, which is the dimensionless boundary to the Bennett Vortex.

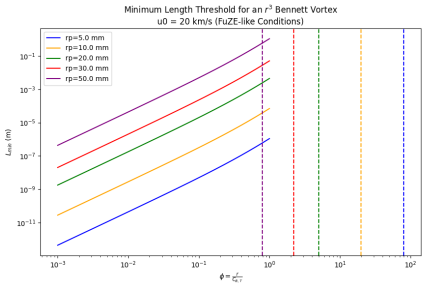

Figure 27. Minimum length required for an r^3 Bennett Vortex to be SFS for FuZE-like conditions with an edge flow speed of $u_{z,0} = 20$ $[km\ s^{-1}]$. Each colored vertical line is the corresponding location of ϕ_p, which is the dimensionless boundary to the Bennett Vortex.

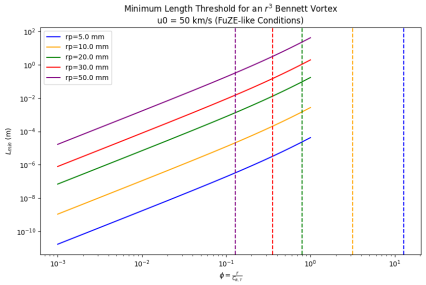

Figure 28. Minimum length required for an r^3 Bennett Vortex to be SFS for FuZE-like conditions with an edge flow speed of $u_{z,0} = 50$ $[km\ s^{-1}]$. Each colored vertical line is the corresponding location of ϕ_p, which is the dimensionless boundary to the Bennett Vortex.

Galaxy Filament Formation

The plasma being a circular disk of uniform density, the impact of its gravitational forces measured along the positive half-chord of the pinch cross-section can be calculated analytically by treating the gravitational forces along the cylinder of mass in the classical sense, i.e., as if all the mass in a given shell were concentrated at the

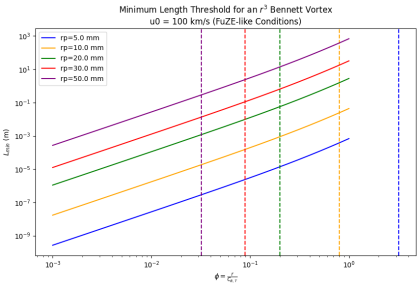

Figure 29. Minimum length required for an r^3 Bennett Vortex to be SFS for FuZE-like conditions with an edge flow speed of $u_{z,0} = 100$ $[km\ s^{-1}]$. Each colored vertical line is the corresponding location of ϕ_p, which is the dimensionless boundary to the Bennett Vortex.

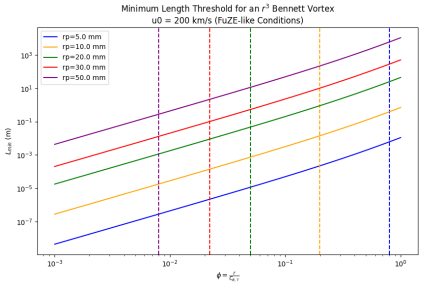

Figure 30. Minimum length required for an r^3 Bennett Vortex to be SFS for FuZE-like conditions with an edge flow speed of $u_{z,0} = 200$ $[km\ s^{-1}]$. Each colored vertical line is the corresponding location of ϕ_p, which is the dimensionless boundary to the Bennett Vortex.

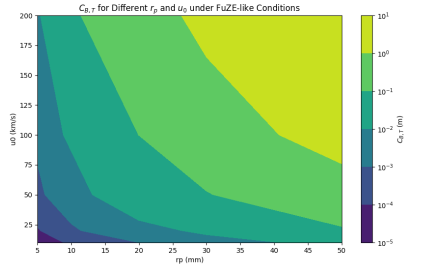

Figure 31. Range of $C_{B,T}$ across the FuZE conditions visualized earlier.

center of the plane, and a central-force was pulling on the test mass, m, of plasma at some point, r. The mass M of the shell is given by,

$$M = 2\pi L \int_0^r r' \rho dr' \tag{109}$$

$$= L\pi r^2 m n_0 \tag{110}$$

and the gravitational force on the test mass, m, in the lab frame,

$$\vec{F}_G = -\frac{GM(r)m}{r^2}\hat{r} \tag{111}$$

The ratio of the gravitational force to the electromagnetic forces felt by the test plasma mass in the lab frame can be calculated for the case $T(r) = C_T r^3$ since the entire equilibrium of a Bennett Vortex can be for this situation. The radial electric field felt by the test plasma mass in its rest frame can necessarily be obtained as well, from Equation (16),

$$\vec{E} = E_r \hat{r} = \frac{r}{(r + C_{B,T})^3} \mu_0 e n_0 u_{z,0}^2 f(r, C_{B,T}) \tag{112}$$

If we use this electric field in a naive attempt to calculate the ratio of these two forces we will find that the electromagnetic force is considered to have no impact on the dynamics of the plasma mass, and this is by definition. Instead, we boost to a lab frame travelling at a velocity, $\vec{u}_{lab}$,

$$\vec{u}_{lab} \times \vec{B} = -2\vec{u} \times \vec{B} \tag{113}$$

$$\therefore \vec{u}_{lab} = -2\vec{u} \tag{114}$$

Doing so amounts to finding a frame of reference where the electric force adds constructively with the magnetic force instead of cancelling it out fully, as is done in the rest frame of the plasma. Critically, the system remains axisymmetric from this new frame of reference,

$$z_{lab} = z - 2u_z(r)t \tag{115}$$

$$\therefore \frac{\partial q(r)}{\partial z_{lab}} = \frac{\partial z}{\partial z_{lab}} \frac{\partial q}{\partial z} = \frac{\partial q}{\partial z} = 0 \tag{116}$$

and furthermore, this frame of reference is also inertial as the plasma flow is steady. In principle any scaling factor could be coupled to the boost for performing this calculation, subsequently changing the value of the electromagnetic forces seen by the lab observer, but doing so would cause the amplitude of the lab electric field to grow or shrink from its value in the rest frame of the plasma. Furthermore, applying too large a scaling factor, or consider too large an edge flow speed, and the relativistic effects on the observed mass from the lab frame will need to be addressed.

When measured in this frame, the electric field experienced by the plasma mass becomes,

$$\vec{E}_{lab} = \vec{u} \times \vec{B} \tag{117}$$

and the electromagnetic forces in the lab frame become,

$$\vec{F}_{L,lab} = e(\vec{E}_{lab} + \vec{u} \times \vec{B}) \tag{118}$$

$$= 2e(\vec{u} \times \vec{B}) \tag{119}$$

$$= F_{L,lab,r} \hat{r} \tag{120}$$

$$= -2eu_z B_\theta \hat{r} \tag{121}$$

Defining the ratio of the gravitational force to this lab electromagnetic force as,

$$\eta_{GL} = \frac{\int_V |\vec{F}_G(r)| dV}{\int_V |\vec{F}_{L,lab}(r)| dV} = \frac{I_G}{I_{EM}} \tag{122}$$

we have, first, the electromagnetic integral,

$$I_{EM} = 2\pi L e^2 u_{z,0}^2 n_0 \mu_0 \int_0^r \frac{f(r', C_{B,T})}{(1 + \xi^2 r'^2)^4 (r' + C_{B,T})} dr'$$

$$= 2\pi L e^2 u_{z,0}^2 n_0 \mu_0 (L_1 + L_2 + L_3 + L_4) \tag{123}$$

where,

$$L_1 = \int_0^r \frac{f_1(r', C_{B,T})}{(1 + \xi^2 r'^2)^4 (r' + C_{B,T})} dr' \tag{124}$$

$$L_2 = \int_0^r \frac{f_2(r', C_{B,T})}{(1 + \xi^2 r'^2)^4 (r' + C_{B,T})} dr' \tag{125}$$

$$L_3 = \int_0^r \frac{f_3(r', C_{B,T})}{(1 + \xi^2 r'^2)^4 (r' + C_{B,T})} dr' \tag{126}$$

$$L_4 = \int_0^r \frac{f_4(r', C_{B,T})}{(1 + \xi^2 r'^2)^4 (r' + C_{B,T})} dr' \tag{127}$$

These integrals, Equations (124) - (127), are solved using the Wolfram Mathematica CAS, and are fully enumerated in Appendix B. What is important is their leading order when added together,

$$I_{EM} \sim \frac{r^7}{(r + C_{B,T})^4} \sim r^3 \tag{128}$$

and the leading order of the gravitational integral,

$$I_G = 2\pi L G m \int_0^r \frac{1}{r'} M(r') dr' \tag{129}$$

$$= 2\pi^2 L^2 G m^2 n_0 \int_0^r r' dr' \tag{130}$$

$$= (\pi^2 L^2 G m^2 n_0) r^2 \tag{131}$$

Together we find that the ratio, Equation (122) is then given by,

$$\eta_{GL} \sim \frac{L^2 r^2}{L r^3} \sim \frac{L}{r} \tag{132}$$

for this particular, non-relativistic, case where $T = C_T r^3$. On the surface this suggests that in the infinite length limit the gravitational force will dominate, which is to be expected as the gravitational impact on the plasma shell scales with L^2. However, the pinch radius, r_p, which shows up in the theory as the point at which the plasma state jumps to vacuum, can be expressed as a ratio of the major axis,

$$r_p = R_a L \tag{133}$$

where R_a is the aspect ratio of the cylindrical equilibrium. Then, it is the aspect ratio which matters,

$$\eta_{GL}(r_p) \sim \frac{1}{R_a} \tag{134}$$

For the r^3 temperature this still implies that the gravitational force dominates the dynamics of the non-relativistic theory for small aspect ratios. However, for aspect ratios greater than one the electromagnetic force does instead although this also runs counter to the central idea of an extremely long plasma in this classical, non-relativistic limit, and indeed plasma pinches themselves which are small aspect ratio phenomena from the perspective of an inertial lab frame. Consequently, a more detailed calculation using reasonable order of magnitude values is required to clarify the situation. Additionally, different temperature profiles might lead to different η_{GL}, perhaps where the scaling favors the electromagnetic force moreso.

Before leaving this section, there is one final thing that needs to be remarked on in pursuit of this hypothesis, namely, that the edge flow speed can be chosen so that the lab frame is relativistic, in which case the length of the pinch experiences a contraction, paving the way for a coherent argument founded on a large aspect ratio pinch. From the perspective of the cosmic web electrons, or even the ions, it is very possible for the microscopic description to be relativistic. The ideal theory of relativistic magnetofluids grows substantially more complicated[18], and is therefore outside the scope of this work.

Kadomtsev Stability

A Z-pinch can be made stable to the $m = 0$ mode by tailoring the pressure profile in a certain way as B.B. Kadomtsev discovered[19]

$$-\frac{\mathrm{d}\ln(p)}{\mathrm{d}\ln(r)} \geq \frac{4\Gamma}{2+\Gamma\beta} \tag{135}$$

which can be manipulated into the form,

$$B^2 \leq -\frac{\mu_0\Gamma p}{2\Gamma + \frac{\mathrm{d}\ln(p)}{\mathrm{d}\ln(r)}}\frac{\mathrm{d}\ln(p)}{\mathrm{d}\ln(r)} \tag{136}$$

for $\beta = \frac{2\mu_0 p}{B^2}$. For $T = C_T r^3$ the above can be written as,

$$B^2 + \frac{3\mu_0\Gamma(n_0 k_B C_T)^2}{2\Gamma + 3n_0 k_B C_T} r^3 \leq 0 \tag{137}$$

evidently leaving only one possible path forward in pursuing the above line of attack, since both B^2, and the cubic term are positive-definite for $C_T > 0$. Namely, finding roots to the equation,

$$B^2(r) + \frac{3\mu_0\Gamma(n_0 k_B C_T)^2}{2\Gamma + 3n_0 k_B C_T} r^3 = 0 \tag{138}$$

which for the specific case of $T = C_T r^3$ can be represented by,

$$\frac{\mu_0^2 e^2 n_0^2 u_{z,0}^2}{2r^2(r + C_{B,T})^2} f^2 + \frac{3\mu_0\Gamma(n_0 k_B C_T)^2}{(2\Gamma + 3n_0 k_B C_T)} r^3 = 0 \tag{139}$$

where f is described by (60). The highest-order in f^2 is sixth, however, the denominator attached to f^2 has fourth-order terms lurking which must be multiplied through, leading to,

$$r^7 + \mu_0 e^2 u_{z,0}^2 (\frac{\Gamma + 3n_0 C_T k_B}{6\Gamma k_B^2 C_T^2}) f^2(r, C_{B,T}) + 2C_{B,T} r^6 + C_{B,T}^2 r^5 = 0$$

the roots of this equation would give relationships amongst the parametric values of the model that represent states where the Kadomtsev condition is exactly met. No analytic formula is, or can be, known for root-finding with arbitrary coefficients for polynomials of degree greater than or equal to 5[20]. Therefore, roots to Equation (139) would need to be found numerically. This computation is of interest as these roots describe Bennett Vortices which are also at the very limit of what Kadomtsev stability to the $m = 0$ mode would accept.

FUTURE WORK AND CONCLUSION

The pure-flow Bennett Vortex expresses a valid SFS Z-pinch equilibrium in the ideal limit, $R_m \to \infty$, via way of $L \to \infty$, when the plasma temperature can be written as,

$$T(r) = a_n r^n \tag{140}$$

with,

$$n > 2 \tag{141}$$

In the specific case when,

$$T(r) = C_T r^3 \tag{142}$$

with

$$C_T = \frac{T(r_p)}{r_p^3} \tag{143}$$

then the azimuthal magnetic field can be solved for analytically to verify that the ideal limit of the shear threshold converges to zero in the case of uniform density, and that the flow shear theoretically satisfies this condition everywhere in the pinch cross-section.

When compared to experimental results from contemporary SFS machines, the theory of an r^3 Bennett Vortex compares favorably. Most notably it predicts the peak shear in a FuZE-like device to very close agreement with measured shear data, and possesses an axial velocity profile that appears locally in the measured axial velocity profile of real SFS Z-Pinches. Additionally, its magnetic field has a similar structure to the observed magnetic field in real SFS Z-Pinches, namely that of a null at the axis and a maximum at the pinch radius. These match with the understood notions of what Ideal MHD is good for predicting, namely the influence of magnetic geometry

on the equilibrium and stability of a plasma. Furthermore, for small pinch radii, the predictions made by the theory of an r^3 Bennett Vortex give order-of-magnitude agreement with the experimental data for magnetic field strength, enclosed current, and pressure drop.

This is all very curious as the temperature gradient of an r^3 Bennett Vortex points in the opposite direction when compared to the observed electron temperature profile seen in experiments, which looks like an upside-down parabola. However, the length scale over which an r^3 Bennett Vortex can form an SFS state for FuZE-like conditions can be very small.

Indeed, when considering how the lower bound on the pinch length necessary for a pure-flow cubic vortex to qualify as an SFS state varies with distance from the pinch axis it is found that,

$$\tilde{L}_2(0) = \lim_{\phi \to 0} \tilde{L}_2(\phi) = 0 \tag{144}$$

implying that cubic vortices forming arbitrarily close to the pinch axis can assume SFS states for arbitrarily small pinches.

In this vein, the appearance of localized r^3, pure-flow, Bennett Vortices can be seen in the axial velocity data of real SFS experiments, although the author has not yet been privileged access to this data for calculating a quantitative fit. In conjunction with the calculated lower bound on the lengths required for these structures to be SFS it is reasonable to conclude that r^3 Bennett Vortices are found in these real SFS experiments, and will be found at some scale, for any SFS Z-Pinch plasma as they can form arbitrarily short SFS states arbitrarily close to the pinch axis so they are undoubtedly going to be mixed into any SFS Z-Pinch plasma.

The system of the pure-flow r^3 Bennett Vortex is readily extensible to study an analytic model based on the experimentally observed uniform line source of fusion neutrons located on the axis of the pinch, because the uniform density does not alter the structure of the magnetic field which will still be analytic, and will instead be a source of energy that influences the background of the plasma. This model will still be of limited use however, beyond making accurate predictions regarding the shear, and order of magnitude estimates of the other quantities. It will however serve appropriately as an analytic model of an SFS fusion plasma which can be used to design both a fusion plasma reactor based on the idea, and a fusion rocket. Most importantly this can be used to inform how the plasma will perform at extremely large current approaching the Kruskal-Shafranov limit.

There are also other flavors of Bennett Vortex to consider, beyond just the changing the form of the temperature profile. For example, the nonlinearity can be mixed between the plasma number density, and plasma flow, and so long as the Bennett current maintains the same form as for an r^3-vortex, then the magnetic field will retain the same structure irrespective of how the nonlinearity is partitioned between the flow and density. This provides a theoretical way to study the impact of increasing the shear of the device, as well as the impact on plasma performance from having different ratios of density and flow speed. This also provides a potential avenue for explaining the structures that form during later pulses which are not of the same form as the pure-flow cubic vortex.

Comments have already been made about interpreting the core experimental temperature as the edge plasma temperature in the analysis of an r^3 Bennett Vortex, but they must be made again in regards to the edge plasma flow, which is related to $u_{z,0}$, but not strictly the same thing except when $C_{B,T}$ is very small, and/or the pinch radius is very large.

A simulation of this analytic SFS equilibrium is also necessary as a next step in studying it. To examine the galaxy filament hypothesis in greater detail, and also to study fusion plasmas with relativistic flow speeds, a relativistic theory of the r^3 Bennett Vortex should be formulated. Lastly, different temperature profiles can also be studied as some of them will perhaps have analytic solutions as well.

ACKNOWLEDGEMENTS

The author would like to acknowledge Uri Shumlak for discovering the SFS Z-Pinch, Eric Meier for inspiring the study of the Bennett Pinch, Aria Johansen for her supportive comments and insightful feedback on the early manuscript, Iman Datta for his insights on Ideal MHD, Jeff Peachman, and Jack Coughlin for their support and feedback, Daniel Crews for his feedback on the early manuscript, and Whitney Thomas for her patience.

APPENDIX A: BASE-FLOW, CUBIC, PLASMA PRESSURE INTEGRALS

The Mathematica notebook that evaluated these integrals can be found here.

$$\begin{aligned} P_2 = \frac{1}{4} u_0 u_{z0} \Bigg\{ & r^2 - 8 r C_{B,T} \\ & - 2 C_{B,T}^2 \Bigg[\pi^2 - 6 \operatorname{arctanh}\left(\frac{r}{r + 2C_{B,T}} \right) \\ & + 5 \ln\left(1 + \frac{r}{C_{B,T}} \right) + 6 \ln\left(r \left(1 + \frac{r}{C_{B,T}} \right) \right) \ln(C_{B,T}) \\ & + 6 i \pi \ln\left(\frac{C_{B,T}}{r + C_{B,T}} \right) - 6 \ln(r) \ln(r + C_{B,T}) \\ & - 6 \operatorname{Li}_2\left(1 + \frac{r}{C_{B,T}} \right) \Bigg] \Bigg\} \end{aligned} \tag{145}$$

where $Li_2(1+\frac{r}{C_{B,T}})$ is the second-order Jonquiere function (polylogarithm).

$$P_4 = \frac{u_{z0}^2}{4(r+C_{B,T})^2}\Bigg\{r^4 + C_{B,T}\Bigg[-10r^3 \tag{146}$$
$$+ 3C_{B,T}r^2\Bigg(-13 + 2\ln^2(C_{B,T})$$
$$+ 2\ln(r+C_{B,T})\Big[3+\ln(r+C_{B,T})\Big]$$
$$- 2\ln(C_{B,T})\Big[3+2\ln(r+C_{B,T})\Big]\Bigg)$$
$$+ 2C_{B,T}r\Bigg(\Big[-5+2\ln^2(C_{B,T})$$
$$- 4\ln(C_{B,T})\Big(2+\ln(r+C_{B,T})\Big)$$
$$+ 2\ln(r+C_{B,T})\Big(4+\ln(r+C_{B,T})\Big)\Big]$$
$$+ C_{B,T}\ln\left(1+\frac{r}{C_{B,T}}\right)\left[5+\ln\left(1+\frac{r}{C_{B,T}}\right)\right]\Bigg)\Bigg]\Bigg\}$$

APPENDIX B: I_{EM} INTEGRALS

The net electromagnetic impulse provided to the plasma, from the frame of reference where,

$$\vec{E} = \vec{u}\times\vec{B} \tag{147}$$

which requires boosting to a frame that is travelling at a velocity,

$$\vec{u}_{lab} = -2\vec{u} \tag{148}$$

relative to the rest frame of the plasma flow, which itself is travelling at a velocity,

$$\vec{u} = \frac{u_{z,0}}{(1+\xi^2r^2)^2}\hat{z} \tag{149}$$

is calculated from,

$$I_{EM} = \int_V |\vec{F}_{L,lab}|dV \tag{150}$$
$$= 2\pi e^2 u_{z,0}^2 n_0\mu_0 L\int_0^r \frac{f(r',C_{B,T})}{(1+\xi^2r'^2)^4(r'+C_{B,T})}dr' \tag{151}$$

where,

$$f(r,C_{B,T}) = f_1+f_2+f_3+f_4 \tag{152}$$

with,

$$f_1(r) = r^3 \tag{153}$$
$$f_2(r,C_{B,T}) = -3r^2C_{B,T} \tag{154}$$
$$f_3(r,C_{B,T}) = -6rC_{B,T}^2(1+\ln\Big(\frac{C_{B,T}}{r+C_{B,T}}\Big)) \tag{155}$$
$$f_4(r,C_{B,T}) = -6C_{B,T}^3\ln\Big(\frac{C_{B,T}}{r+C_{B,T}}\Big) \tag{156}$$

so that we write I_{EM} as,

$$I_{EM} = 2\pi e^2u_{z,0}^2n_0\mu_0L(L_1+L_2+L_3+L_4) \tag{157}$$

with,

$$L_1 = \int_0^r \frac{f_1(r',C_{B,T})}{(1+\xi^2r'^2)^4(r'+C_{B,T})}dr' \tag{158}$$
$$L_2 = \int_0^r \frac{f_2(r',C_{B,T})}{(1+\xi^2r'^2)^4(r'+C_{B,T})}dr' \tag{159}$$
$$L_3 = \int_0^r \frac{f_3(r',C_{B,T})}{(1+\xi^2r'^2)^4(r'+C_{B,T})}dr' \tag{160}$$
$$L_4 = \int_0^r \frac{f_4(r',C_{B,T})}{(1+\xi^2r'^2)^4(r'+C_{B,T})}dr' \tag{161}$$

which are just Equations (124) - (127). These integrals are computed with Wolfram Mathematica, and transcribed to LaTeX using Gemini Pro 3. The Mathematica notebook containing the computed expressions can be found here.

$$L_1 = \frac{1}{12(r+C_{BT})^4}\Bigg[$$
$$4r^7$$
$$- 14C_{BT}r^6$$
$$+ 84C_{BT}^2r^5$$
$$+ 35C_{BT}^3r^4\left(25+12\ln\left(\frac{C_{BT}}{r+C_{BT}}\right)\right)$$
$$+ 140C_{BT}^4r^3\left(13+12\ln\left(\frac{C_{BT}}{r+C_{BT}}\right)\right)$$
$$+ 210C_{BT}^5r^2\left(7+12\ln\left(\frac{C_{BT}}{r+C_{BT}}\right)\right)$$
$$+ 420C_{BT}^6r\left(1+4\ln\left(\frac{C_{BT}}{r+C_{BT}}\right)\right)$$
$$+ 420C_{BT}^7\ln\left(\frac{C_{BT}}{r+C_{BT}}\right)\Bigg]$$

$$L_2 = -\frac{3C_{BT}}{4(r+C_{BT})^4}\Bigg[$$
$$2r^6$$
$$- 12C_{BT}r^5$$
$$+ 5C_{BT}^2r^4\left(-25+12\ln\left(1+\frac{r}{C_{BT}}\right)\right)$$
$$+ 20C_{BT}^3r^3\left(-13+12\ln\left(1+\frac{r}{C_{BT}}\right)\right)$$
$$+ 30C_{BT}^4r^2\left(-7+12\ln\left(1+\frac{r}{C_{BT}}\right)\right)$$
$$- 60C_{BT}^5r\left(1-4\ln\left(1+\frac{r}{C_{BT}}\right)\right)$$
$$- 60C_{BT}^6\ln\left(\frac{C_{BT}}{r+C_{BT}}\right)\Bigg]$$

$$
\begin{aligned}
L_3 = -\frac{C_{BT}^2}{24(r+C_{BT})^4}\Bigg[\quad & 144r^5\left(2+\ln(C_{BT})-\ln(r+C_{BT})\right) \\
& -5r^4C_{BT}\Bigg(-185+72\ln^2(r)-72\ln^2(C_{BT}) \\
& \quad +144\ln(C_{BT})(-2+\ln(r+C_{BT})) \\
& \quad -144\ln(r)(-1+\ln(r+C_{BT}))+144\ln(r+C_{BT}) \\
& \quad +144\ln\left(\frac{r+C_{BT}}{r}\right)-72\ln^2\left(\frac{r+C_{BT}}{r}\right)\Bigg) \\
& +20r^3C_{BT}^2\Bigg(41+72\ln^2(r)+72\ln^2(C_{BT}) \\
& \quad -144\ln(C_{BT})(-1+\ln(r+C_{BT})) \\
& \quad -144\ln(r+C_{BT})+144\ln(r)\ln\left(\frac{r+C_{BT}}{r}\right) \\
& \quad +72\ln^2\left(\frac{r+C_{BT}}{r}\right)\Bigg) \\
& +30r^2C_{BT}^3\Bigg(5+72\ln^2(r)+72\ln^2(C_{BT})-144\ln(r+C_{BT}) \\
& \quad -72\ln(C_{BT})(-1+2\ln(r+C_{BT})) \\
& \quad +72\ln\left(\frac{r+C_{BT}}{r}\right)+72\ln^2\left(\frac{r+C_{BT}}{r}\right) \\
& \quad +72\ln(r)\left(1+2\ln\left(\frac{r+C_{BT}}{r}\right)\right)\Bigg) \\
& +60rC_{BT}^4\Bigg(-1+24\ln^2(r)+24\ln^2(C_{BT}) \\
& \quad +\ln(C_{BT})(8-48\ln(r+C_{BT}))-48\ln(r+C_{BT}) \\
& \quad +40\ln\left(\frac{r+C_{BT}}{r}\right)+24\ln^2\left(\frac{r+C_{BT}}{r}\right) \\
& \quad +8\ln(r)\left(5+6\ln\left(\frac{r+C_{BT}}{r}\right)\right)\Bigg) \\
& +60C_{BT}^5\Bigg(6\ln^2(C_{BT})+\ln(r+C_{BT})(1+6\ln(r+C_{BT})) \\
& \quad -\ln(C_{BT})(1+12\ln(r+C_{BT}))\Bigg)\Bigg]
\end{aligned}
$$

$$
\begin{aligned}
L_4 = -\frac{C_{BT}^3}{24(r+C_{BT})^4}\Bigg[\quad & r^4\left(415-72\ln^2\left(\frac{C_{BT}}{r+C_{BT}}\right)\right) \\
& +4r^3C_{BT}\left(271+144\ln\left(\frac{C_{BT}}{r+C_{BT}}\right)-72\ln^2\left(\frac{C_{BT}}{r+C_{BT}}\right)\right) \\
& +6r^2C_{BT}^2\left(163+216\ln\left(\frac{C_{BT}}{r+C_{BT}}\right)-72\ln^2\left(\frac{C_{BT}}{r+C_{BT}}\right)\right) \\
& -12rC_{BT}^3\left(-25-88\ln\left(\frac{C_{BT}}{r+C_{BT}}\right)+24\ln^2\left(\frac{C_{BT}}{r+C_{BT}}\right)\right) \\
& +12C_{BT}^4\ln\left(\frac{C_{BT}}{r+C_{BT}}\right)\left(25-6\ln\left(\frac{C_{BT}}{r+C_{BT}}\right)\right)\Bigg]
\end{aligned}
$$

[1] J. Allen and L. Simons, The bennett pinch for non-relativistic electrons, J. Plasma Phys., vol. 84 (2018).

[2] W. H. Bennett, Magnetically self-focussing streams, Physical Review, Volume 45 (1934).

[3] U. Shumlak, Z-pinch fusion, Journal of Applied Physics **127**, 200901 (2020), https://pubs.aip.org/aip/jap/article-pdf/doi/10.1063/5.0004228/20006426/200901_1_5.0004228.pdf.

[4] U. Shumlak and C. W. Hartman, Sheared flow stabilization of the $m = 1$ kink mode in Z pinches, Phys. Rev. Lett. **75**, 3285 (1995).

[5] U. Shumlak, R. P. Golingo, B. A. Nelson, and D. J. Den Hartog, Evidence of stabilization in the Z-pinch, Phys. Rev. Lett. **87**, 205005 (2001).

[6] U. Shumlak, B. A. Nelson, R. P. Golingo, S. L. Jackson, E. A. Crawford, and D. J. Den Hartog, Sheared flow stabilization experiments in the zap flow z pinch, Physics of Plasmas **10**, 1683 (2003), https://pubs.aip.org/aip/pop/article-pdf/10/5/1683/19271537/1683_1_online.pdf.

[7] R. P. Golingo, U. Shumlak, and B. A. Nelson, Formation of a sheared flow Z pinch, Physics of Plasmas **12**, 062505 (2005).

[8] D. J. Ampleford, S. N. Bland, M. E. Cuneo, S. V. Lebedev, D. B. Sinars, C. A. Jennings, E. M. Waisman, R. A. Vesey, G. N. Hall, F. Suzuki-Vidal, J. P. Chittenden, and S. C. Bott, Demonstration of radiation pulse-shaping capabilities using nested conical wire-array z-pinches, IEEE Transactions on Plasma Science **40**, 3334 (2012).

[9] U. Shumlak, B. Nelson, and B. Levitt, The sheared-flow-stabilized z-pinch approach to fusion energy, in *2023 IEEE International Conference on Plasma Science (ICOPS)* (2023) pp. 1–1.
[10] P. Davidson, *Introduction to Magnetohydrodynamics* (Cambridge University Press, 2017).
[11] P. Davidson, *Turbulence* (Cambridge University Press, 2015).
[12] J. P. Friedberg, *Ideal MHD* (Cambridge University Press, 2014).
[13] J. Huba, *NRL Plasma Formulary* (Naval Research Laboratory, 2013).
[14] U. Shumlak, C. S. Adams, J. M. Blakely, B. J. Chan, R. P. Golingo, S. D. Knecht, B. A. Nelson, R. J. Oberto, M. R. Sybouts, and G. V. Vogman, Equilibrium, flow shear and stability measurements in the Z-pinch, Nuclear Fusion **49**, 075039 (2009).
[15] E. T. Meier and U. Shumlak, Development of five-moment two-fluid modeling for z-pinch physics, Physics of Plasmas **28**, 092512 (2021), https://pubs.aip.org/aip/pop/article-pdf/doi/10.1063/5.0058420/13420598/092512_1_online.pdf.
[16] D. W. Crews, I. A. M. Datta, E. T. Meier, and U. Shumlak, The kadomtsev pinch revisited for sheared-flow-stabilized z-pinch modeling, IEEE Transactions on Plasma Science **52**, 4804 (2024).
[17] J. P. Freidberg, *Plasma Physics and Fusion Energy* (Cambridge University Press, 2007).
[18] A. M. Anile, *Relativistic Fluids and Magneto-fluids: With Applications in Astrophysics and Plasma Physics*, Cambridge Monographs on Mathematical Physics (Cambridge University Press, 1990).
[19] B. Kadomtsev *et al.*, Hydromagnetic stability of a plasma, Reviews of plasma physics **2**, 153 (1966).
[20] P. Ruffini, *Riflessioni intorno alla soluzione delle equazioni algebraiche generali* (Presso La Società, 1813).